Project No. 01-59

PROPOSED ENHANCEMENTS TO PAVEMENT ME DESIGN: IMPROVED CONSIDERATION OF THE INFLUENCE OF SUBGRADE SOILS SUSCEPTIBLE TO SHRINK/SWELL AND/OR FROST HEAVE ON PAVEMENT PERFORMANCE

APPENDIX 3

LABORATORY MEASUREMENTS TO PREDICT STRAIN DUE TO THE SIMULTANEOUS APPLICATION OF SUCTION AND NET NORMAL STRESSES FOR COMPACTED EXPANSIVE SOILS

MAY 2023

TABLE OF CONTENTS

LIST OF FIGURES

LIST OF TABLES

3.1. Abstract

Over the years, several methods to estimate volume change due to expansive soils behavior have been proposed. Some of those studies focused on the suction effect on volume change, using the suction compression index (Lytton et al., 2005), without taking into consideration the effect of the net normal stress. Others, on the other hand, considered both the net normal stress and the suction stress but in an uncoupled fashion. That is, performing a 1-D consolidation test for a fully saturated sample to estimate the mean principal stress compression index, γ_σ, and then performing a soil-water characteristic curve test to estimate the suction compression index, γ_h (Fredlund and Morgenstern, 1976; Fredlund and Rahardjo, 1993).

This document presents the laboratory research work performed to estimate the volume change of compacted specimens due to the application of a coupled net normal and suction stress condition. The results were used to propose a model for estimating volume change of soils for a wide range of expansion potential.

A 1-D oedometer-type pressure plate device (SWC-150) was used for the laboratory testing. This device allows for the application of net normal stress while following various applied matric suctions. Volume changes due to both stresses can be measured and/or calculated in a coupled manner.

Three fine-grained soils, with varying expansion potentials, were used in this analysis. The weighted plasticity index, as defined by Zapata (1999), of the three soils tested were approximately 10, 30, and 50. The suction compression index was measured under drying conditions and an empirical relationship between changes of void ratio, matric suction, net normal stress, and *w*PI was developed. The results of this study greatly enhance the prediction of strains due to suction changes and allow for the evaluation of coupled effects when net normal stresses are simultaneously acting on the soil material.

3.2. Objective

A comprehensive laboratory program was completed using the SWC-150 device that allowed for the performance of both oedometer-type and soil-water characteristic curve (SWCC) tests to measure compression indices at different suction and net normal stress conditions for compacted expansive soils. The results were used to find an empirical correlation that predicts volume change at different suction and net normal stress levels.

3.3. Introduction

Soil suction, Ψ, is one of the primary variables required to understand the unsaturated soil behavior (Fredlund, 2012). It can be defined as the negative pressure created between soil particles when moisture is reduced. Soil suction is widely used, sometimes with other soil and/or environmental parameters, to estimate heave/shrinkage potential (Randy Rainwater et al., 2012). However, measuring soil suction in the laboratory and in the field is difficult and time consuming (Fredlund, 2012).

The soil water characteristic curve, SWCC, is defined as the relationship between soil suction and moisture content, ω. This relationship is usually obtained ***without*** considering volume changes due to the applied

suction. However, "the volume change occurring when drying a clayey soil can be substantial and is relevant to the interpretation of SWCC data (Fredlund, 2012)". Because it is difficult to measure, volume change is usually ***estimated*** using the soils shrinkage curve (SSC), which is the relationship between void ratio, e, and moisture content from fully saturation to completely dry condition under ***free external stress*** (Fredlund, 2012, and Chen and Lu, 2018). Knowing the volume change during the drying process can assist in developing void ratio and soil suction relationship. Void ratio, moisture content, and soil suction in addition to the specific gravity are the key parameters to calculate strain and degree of saturation, which are essential in describing the volume change behavior in unsaturated soils.

The other stress that affects the heave/shrinkage potential is the net normal stress, σ_n. As widely known by the geotechnical engineering community, the change in volume due to the σ_n can be measured in the lab using the oedometer, or consolidometer, testing procedure. A void ratio, or strain, and net normal stress relationship for ***a fully saturated soil*** is the outcome of this lab test.

In nature, suction and net normal stresses act simultaneously while in the lab their effects on volume change are measured separately. In this lab study, both stresses, Ψ and σ_n, were applied together and the volume change was measured to develop void ratio, e, strain, $\boldsymbol{\varepsilon}$, and degree of saturation, S, relationships for three compacted soils with different expansion/shrinkage potentials, as estimated by their weighted plasticity index, *w*PI, of 10, 30, and 50. The *w*PI is defined as the product of Plasticity Index, PI, in percentage multiplied by passing #200 sieve in decimals (Zapata, 1999).

$$wPI = \left(\frac{P_{200}}{100}\right) \times PI \qquad (3-1)$$

This laboratory research work is part of the NCHRP 01-59 project entitled "Proposed Enhancements to Pavement ME Design: Improved Consideration of the Influence of Subgrade Soils Susceptible to Shrink/Swell and/or Frost Heave on Pavement Performance." The goal of the analysis presented here is to create an empirical correlation to enhance strain estimations due to suction changes and improve strain profiles affected by overburden pressure. The result correlations are aimed to be integrated with the methodology being developed for the NCHRP 01-59 project to estimate volume change under pavement structures and will greatly facilitate the implementation process.

3.4. Literature Review

Many laboratory tests and different methods have been developed to measure or estimate volume change due to expansive soils. In 2019, Vann presented more than 30 different methods, that comprise water-content based, soil suction- based, oedometer, and empirical methods, to estimate the volume change of expansive soils (Vann, 2019). One of the methods widely used for volume change estimation within the pavement technical community is the Potential Vertical Rise (PVR) published by the Texas Department of Transportation (TxDOT-12-E, 1978), which includes both empirical-based relationships and results from an oedometer test. PVR is defined as the soil potential, with a known density, moisture, and overburden pressure, to swell when exposed to capillary or surface water. This methodology allows for an upper limit estimation of volume change (expansivity). In 2005, the Texas Department of Transportation (TxDOT) updated the approach to determine the volume change of expansive soils using the work of Lytton et al. (2005), which encompassed a suction-based approach. The study concluded that the previous empirical-based approach significantly overestimated the soil heave and did not account for the shrinkage of the soil

during dry climatic periods. The suction-based approach by Lytton et al. (2005) for estimating the volume change of expansive soils, which was adopted by TXDOT and the Post-Tensioning Institute for the design of slabs on ground (PTI, 2004, and PTI, 2008), was the accumulation of efforts of several related studies including: Lytton (1977), McKeen and Hamberg (1981), Holtz and Kovacs (1981), Cover and Lytton (2001), and Lytton et al. (2005). The approach encompasses the volumetric strain caused by changes in both stress states of the soil, matric suction, and net normal stress. The relationship between the change in each stress state and the volumetric strain, referred to as the compression indices, must be directly measured or empirically determined.

Another approach to estimate expansive soil volume change involves the work of Singhal (2011), and Houston and Houston (2017), which use a suction-oedometer-based approach. The method, referred to as the Surrogate Path Method, SPM, by Singhal (2011), uses a response to wetting test (ASTM D4546) and an estimated suction envelope to estimate the volume change of the soil. The special aspect of the Surrogate Path Method is that neither compression indices need to be measured or estimated by the user, as they are already embedded in the procedure. The SPM provides a method for mapping the wetting path in the volume change versus log matric suction plane (for a fixed net normal stress) into the volume change versus log net normal stress plane. Figure 3.1 illustrates the 3-dimensional plot of the SPM (Singhal, 2010), where the matric suction (u_a-u_w) and vertical strain ($\boldsymbol{\varepsilon}$) axes are presented in an arithmetic scale and the net total stress (σ-u_a) axis is presented in a logarithmic scale.

Another approach, developed by Pham and Fredlund in 2011, made used of four different stress path series to develop volume-mass constitutive surfaces for three artificial soils, named sand, silt, and clay. The outlined paths were:

1. Starting as a slurry, the soil was loaded under a constant net normal stress and then dried to 10^6 kPa.
2. Starting as a slurry, the soil was dried to constant suction and then loaded with net normal stress to 10^4 kPa.
3. The soil was dried from slurry, loaded with a constant net normal stress, and then wetted.
4. The soil was dried from slurry, wetted to constant suction, and then loaded with net normal stress to 10^4 kPa.

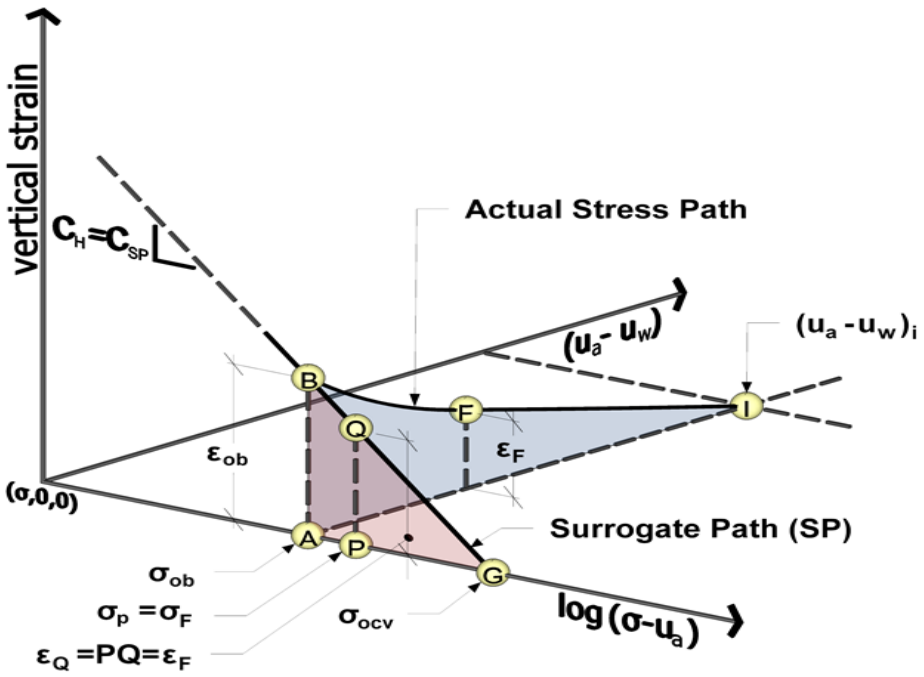

Figure 3.1 Strain-Based "Equivalence" of Reduction of Suction from $(u_a - u_w)_i$ to Zero (Path IB) to Reduction in Net Normal Stress from σ_{OCV} to σ_{ob} (along Path GB, the Surrogate Path) (Vann, 2019)

The study concluded that the stress path affected the results. Figure 3.2 shows the results of the 3 soils for stress path series 1 and 2 only. Figure 3.3 shows the results of the four stress path series for the silt material. It was concluded that the predictions were reasonable and that "the volume-mass constitutive surfaces starting from slurry conditions seem to have steeper slopes than those starting from air-dried conditions" (Pham and Fredlund, 2011).

The following coefficients define the slope of the void ratio versus the respective stress state, (Fredlund et al., 2012)

$$a_t = \frac{\partial e}{\partial(\sigma - u_a)} \; and \; a_m = \frac{\partial e}{\partial(u_a - u_w)} \qquad (3-2)$$

Where,

a_t is the coefficient of compressibility used in the net normal stress slope, and a_m is the coefficient of compressibility used in the matric suction slope, as shown in Figure 3.4.

Similarly, the slope of moisture content versus the respective stress state is defined by the following coefficients,

$$b_t = \frac{\partial w}{\partial(\sigma - u_a)} \; and \; b_m = \frac{\partial w}{\partial(u_a - u_w)} \qquad (3-3)$$

Where,

b_t is the coefficient of compressibility used in the net normal stress slope, and b_m is the coefficient of compressibility used in the matric suction slope, as shown in Figure 3.5.

Constitutive surfaces for silt at low suctions and net mean stresses (stress path series 1 and 2): (*a*) gravimetric water content surface; (*b*) void ratio surface.

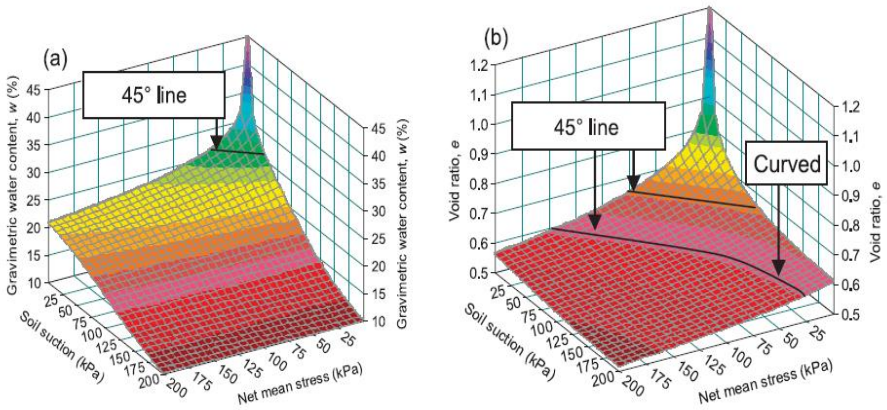

Constitutive surfaces for sand (stress path series 1 and 2 in logarithmic scale): (*a*) void ratio; (*b*) gravimetric water content.

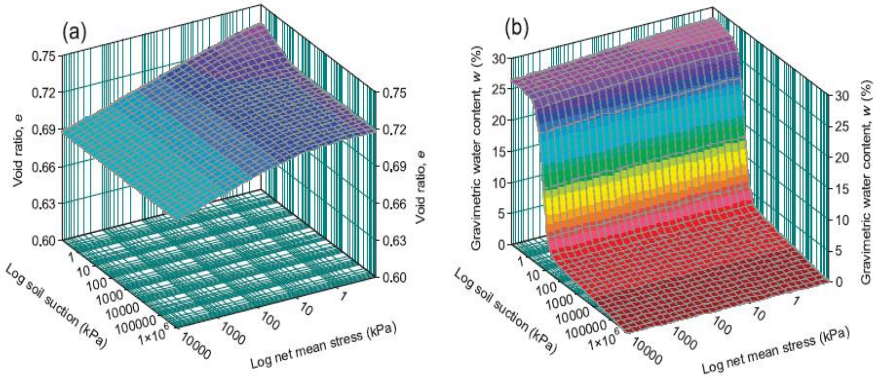

Constitutive surfaces for clay (stress path series 1 and 2 in logarithmic scale): (*a*) void ratio; (*b*) degree of saturation.

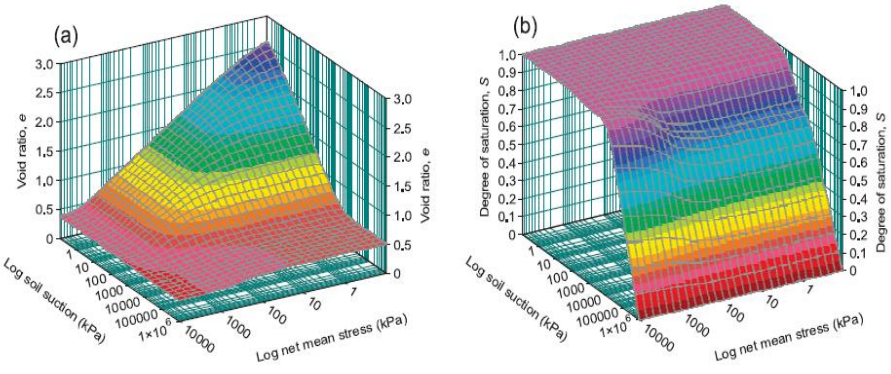

Figure 3.2 Constitutive Surfaces In 3-D For the Three Artificial Soils (Pham and Fredlund, 2011)

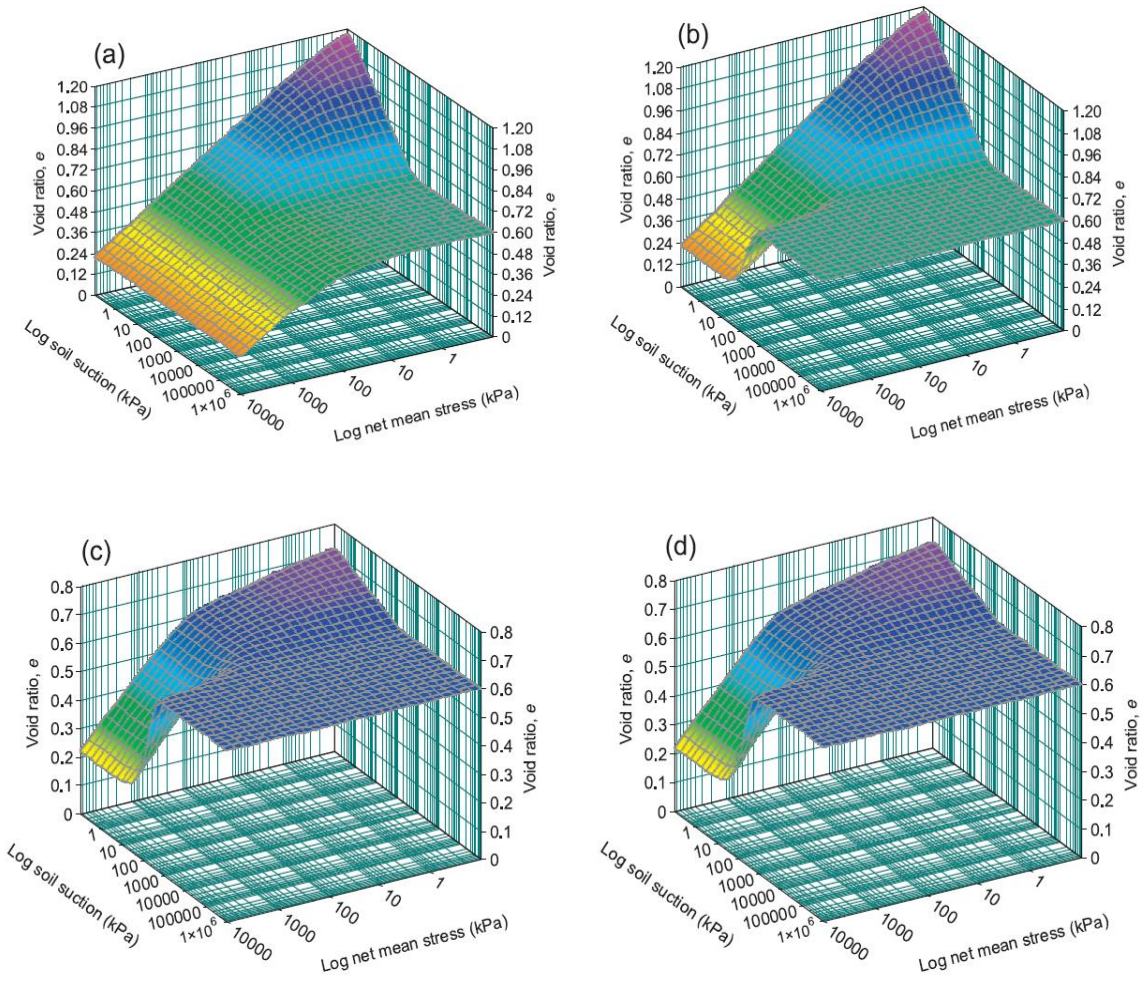

Figure 3.3 Void Ratio Surfaces for Silt for the Four-Stress-Series Respectively (Pham and Fredlund, 2011)

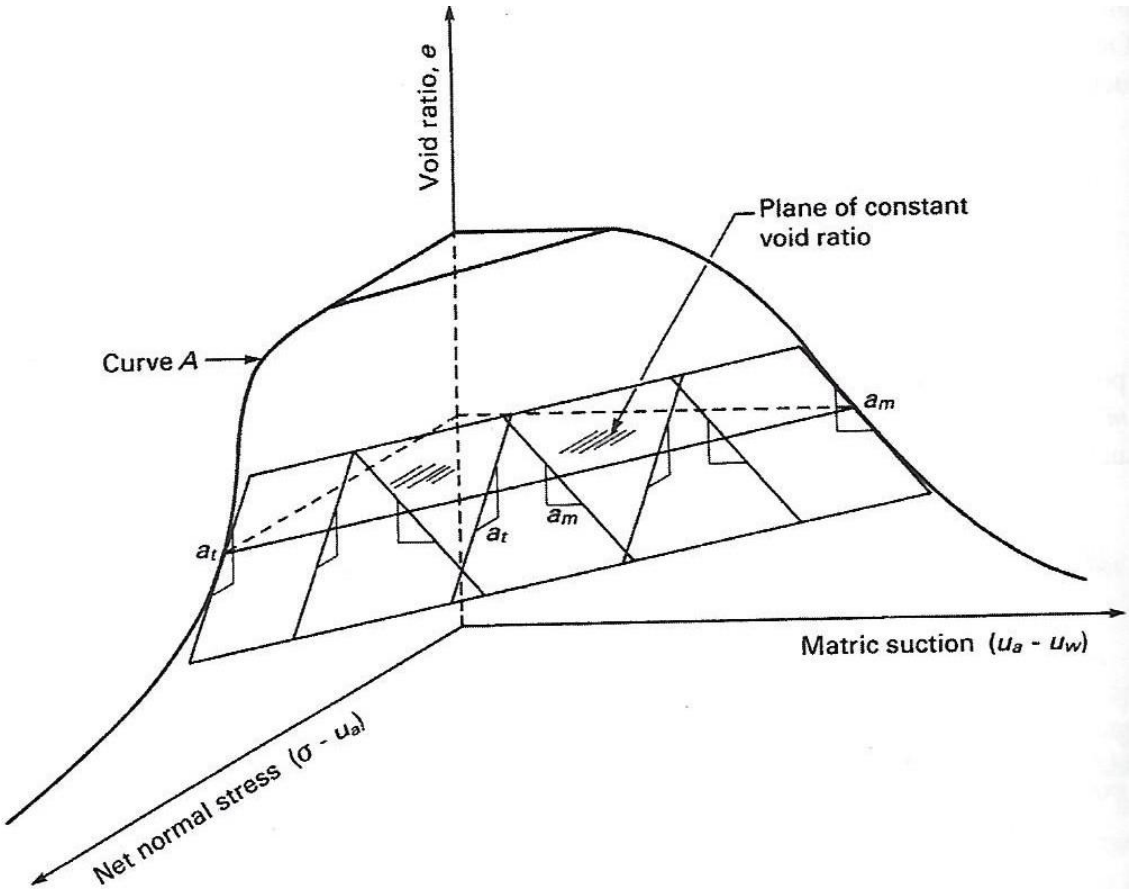

Figure 3.4 Soil Structure Constitutive Surface for Monotonic Loading Assuming Planar Surface at Specific Void Ratio (Fredlund et al., 2012)

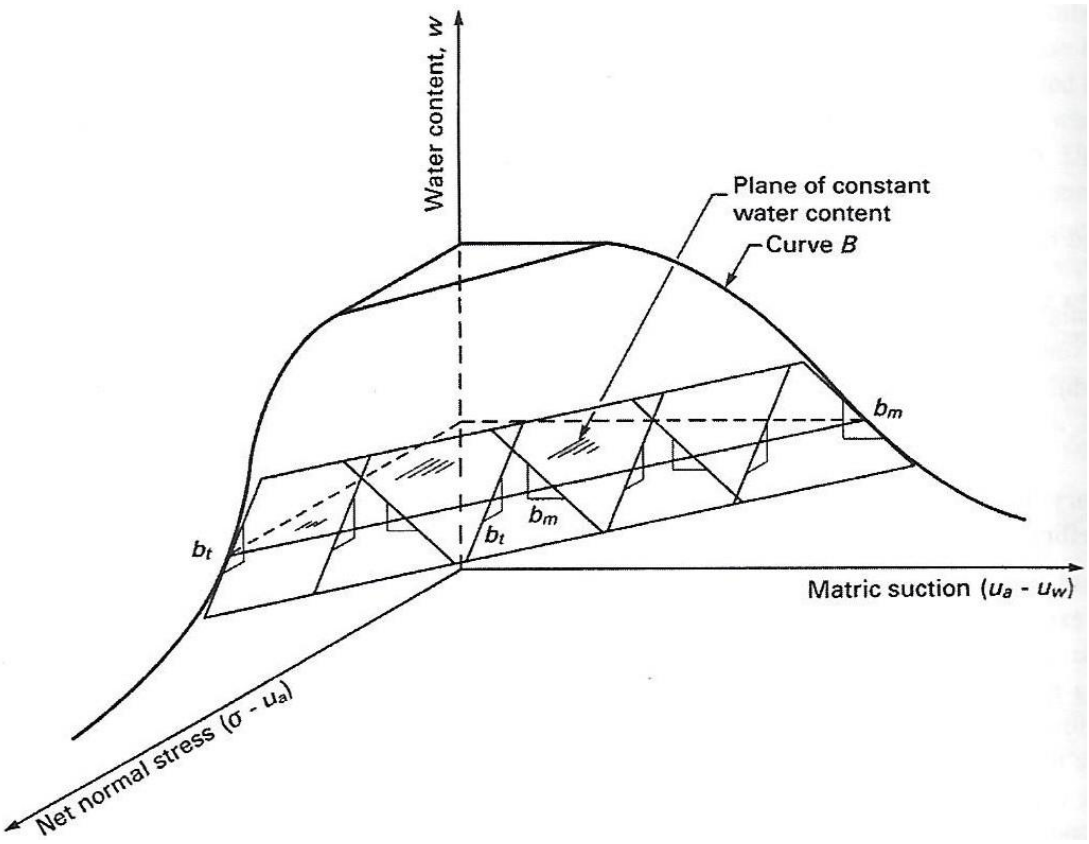

Figure 3.5 Water Phase Constitutive Surface for Monotonic Loading Assuming Planar Surface at Specific Moisture Content (Fredlund et al., 2012)

Curve B in Figure 3.5 is the SWCC and the coefficient b_m is similar to the compression index, C_c, or swelling index C_s depending on how the test is performed.

> *"The a_t, a_m, b_t, and b_m coefficients are used to discuss the relationships that exist between the volumetric deformation coefficients. These coefficients vary from one state point to another along a nonlinear constitutive surface. A direct method to determine these coefficients at a specific state point is to measure their magnitude at the stress point under consideration… Numerous specimens and a long period of testing are generally required to experimentally define the entire constitutive surface"* (Fredlund et al., 2012).

As presented above, the literature reviewed reveals a framework to define the volume change with the suction and net normal stress variables. However, there are no studies that report volume change based on a coupled approach for different soil types.

3.5. Methodology and Material Properties

3.5.1. Methodology

Prediction of volume change under pavement caused by expansive soil behavior is challenging due to the multiple factors that affect the procedure. These factors include climatic boundary conditions and the

climate depth of influence, soil properties, the suction stress state variation, and the applied overburden pressures. The idea of this study is to create a model that can help practitioners in the pavement design field to better estimate volume change due to expansive soil behavior. As a result, the subgrade properties under pavement were used to develop the methodology of this study as follows,

- Soil specimen was compacted at 90% of maximum dry unit weight, $\gamma_{d_{max}}$, at optimum moisture content, ω_{opt}.
- Following Pham and Fredlund (2011) results, stress path 1 was chosen for the analysis to capture the steeper slopes developed when starting from wet condition.
    - The sample was saturated first, consolidated under constant net normal stress, and then dried to 1400 kPa.
- Applied net normal stress varied from 1 to 60 kPa, about 20 to 1250 psf. The maximum was assumed to be a 10-ft-deep point under pavement and *soil* with an average density of 125pcf.

3.5.2. Material Properties

Using *w*PI as a guide to define the expansivity level, the higher the *w*PI value the higher the expansivity level, 3 categories were chosen for the study, 1) *w*PI = 10, 2) *w*PI = 30, and 3) *w*PI = 50. The soils were provided by Vann Engineering Inc. Grain-size distribution and Atterberg limits tests results were available for most of the provided soils. However, some samples were less than 1 kg while for this study at least 2 kg of soil were needed. As a result, some samples were mixed, and soil gradation tests and Atterberg Limits tests were performed for the mixed material. This applies for soils within categories 1 and 2, but not category 3 because a sample with more than 2 kg of soil was found and two soil index properties results were available, as shown in

Table 3.1. The average of the two results was used in the calculations and the analysis. Soil index tests included:

- Wet sieve analysis following ASTM C92-95
- Atterberg Limits, Liquid Limit and Plastic Limit following ASTM D 4318
- Mini compaction following Sridharan and Sivapullaiah procedure (Sridharan and Sivapullaiah 2005)
- Specific gravity (ASTM D 854-02)

Specific gravity test was performed for all the 3 categories since no records were available. A summary of the soil index properties can be found in Table 3.2 and detailed results can be found in Appendix A.

Table 3.1 Soil Index Properties for *Category 3*

Test	% Fines	LL	PL	PI	***w*PI**
1	91	72	18	54	49.1
2	92	70	15	55	50.6

Table 3.2 Summary of Index Properties of Soil Samples Used in The Study

Category	**1**	**2**	**3**
P_4	100	99.3	100
P_{40}	98.8	90.9	100
% Fines (P_{200})	66.5	78.9	91.5
LL	34.5	55.3	71
PL	18	19.7	16.5
PI	17	36	54.5
*w*PI	11.3	28.4	49.9
$\boldsymbol{\omega}_{opt}$ (%)	16.2	21.5	26
$\gamma_{d_{max}}$ (lb/ft^3)	113.5	103.5	90.7
SG	2.71	2.7	2.68

3.6. Sample Preparation

Samples were compacted inside a brass ring at 90% of $\gamma_{d_{max}}$ and at or near the ω_{opt}. To do so, the following steps were followed for each soil category,

- Collect a 1000 g of soil
- Measure the initial room temperature moisture content, ω_0
- Calculate the dry mass as follows

$$M_{dry} = \frac{M_{wet}}{\left(1 + \frac{\omega}{100}\right)} \qquad (3-4)$$

- Calculate the mass of water required to reach the optimum using the following:

$$M_{w_{added}} = \frac{M_{dry} \times \left(\omega_{opt} - \omega_0\right)}{100} \qquad (3-5)$$

- Mix the sample thoroughly and transfer the mixture into a sealed plastic bag back and seal it well and leave it for at least 2 hours. Note that samples were left for 24 hours
- Measure the moisture content, which should be at or near the optimum moisture content
- Using mass, volume, and density relationship, mass of soil required to achieve 0.9 of max dry density was calculated and used
- Results for all samples used in this experimental study can be found in Appendix B

3.7. Test Program

The SWC-150 Fredlund Soil Water Characteristic Device was used for the laboratory testing. This device is capable of tracking moisture content and vertical elevation changes while net normal stress is applied.

3.7.1. Apparatus

Figure 3.6 shows the SWC-150 the Pressure Cell Assembly, Pressure Panel, and the Loading Frame. Different High Air Entry Value, HAVE, ceramic stones available. Table 3.3 is used as a guidance to choose the best ceramic stone based on the soil type (GCTS, 2007).

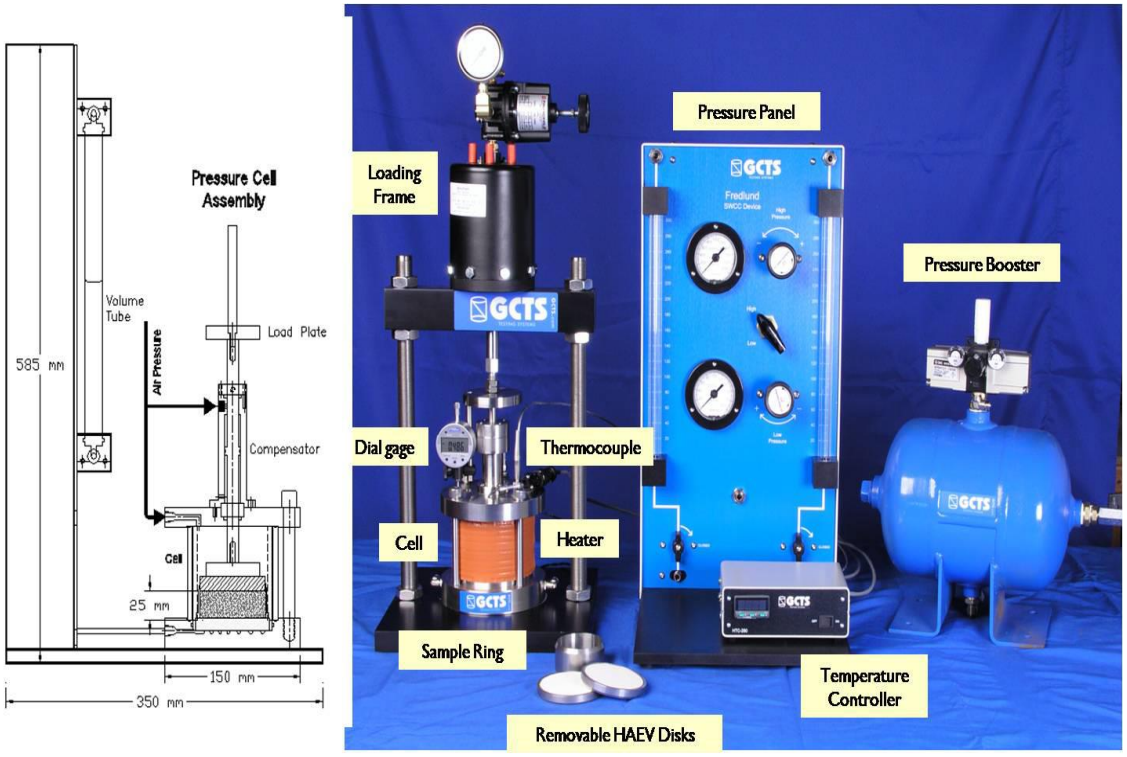

Figure 3.6 SWC-150 Apparatus (GCTS, 2007)

Table 3.3 Selection of Ceramic Stones (GCTS, 2007)

Type of Soil	Rating of Ceramic Stone
Sand	1-bar
Silty Sand, Clayey Sand	3-bar
Sandy Silt, Sandy Clay	5-bar
Clay	15-bar

3.7.2. Procedure

Detailed procedure can be found in the SWC-150 User's Guide & Reference Manual (GCTS, 2007), and Olaiz dissertation (Olaiz, 2017). This procedure is based on the ASTM D6836-16 *Standard Test Methods for Determination of the Soil Water Characteristic Curve for Desorption Using Hanging Column, Pressure Extractor, Chilled Mirror Hygrometer, or Centrifuge*. The following are the steps followed in the lab, which highlights some modifications made to the procedure, that allowed for the simultaneous measurement of the effect of suction and net normal stresses on volume change:

1. Saturate the ceramic stones by placing them under de-aerated water overnight. Before placing them inside the cell, make sure to dry the metal ring and lightly the top and bottom of the ring to have a saturated surface dry (SSD) condition. Then, measure the mass of the stone.
2. Determine the dimensions and the mass of a brass ring. After compacting the soil specimen inside the brass ring at 90% of $\gamma_{d_{max}}$ and ω_{opt}, determine the mass of the soil and the ring.
3. Saturate the specimen following the sketch of Figure 3.7. Because expansive soils are used, expansion due to the increase of moisture content, from optimum to fully saturation, should be measured. Thus, the SWC Cell was used as the container and the dial gauge measured the increase in elevation increase, thus the volume assuming uniform elevation change. Dial gauge reading was measured every 24 hours until no change occurred. Saturating clays might take up to a week, or sometimes even longer, due to the low hydraulic conductivity.

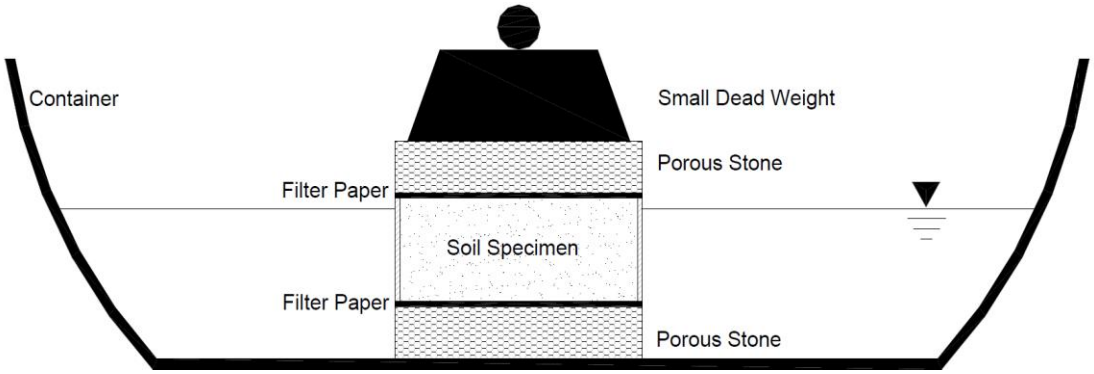

Figure 3.7 Soil Specimen Saturation (GCTS, 2007)

4. Dry the water inside the cell, remove the saturated soil specimen and place it on a glass plate to drain any excess water. Remove the excess water and measure the mass of the soil specimen with the ring.
5. Insert the SSD ceramic stone inside the SWC cell assembly after cleaning the cell from any soil particle. Then add the specimen properly centered on top of the specimen.
6. Then the system can be closed, and the test is ready to run following the procedure of the SWC-150 Manual (GCTS, 2007).
7. *For troubleshooting purposes*, just after closing the system, apply the maximum suction at which the samples will be tested for 1 minute or less and make sure no air leakage exists in the system.
8. Before applying any loads, record the dial gauge reading. Then apply the net normal stress to perform a consolidation test under a constant stress and approximately zero suction. Five machines were used simultaneously, each set at a constant net normal stress applied, 1, 10, 20, 40, or 60 kPa.
9. Take dial gauge and water change readings every 24 hours until no change occurs.
10. Apply suction as needed for the analysis. Record dial gauge and water change measurements every 24 hours until no change occurs neither in dial gauge nor in water level. *Remember to flush for diffused air before taking a reading*. Once equilibrium is achieved, the next suction increment can be applied.
11. Repeat the procedure for the rest of applied suction values.
12. Once reaching the end of the test, a) record final measurements, b) remove loads and release the chamber pressure, c) open the cell and remove the soil sample, d) measure the mass of the soil

and the ring and place in the oven to perform a moisture content test, and e) remove the ceramic stone, bring it to SSD condition and measure its mass. If a significant difference occurs between the initial and final mass of the ceramic stone, volume reading adjustments may be required.

3.8. Calculations

To better explain the calculations process, the test procedure was divided into 3 phases: 1) saturation, 2) consolidation, 3) drying by applying suction. Also, to help understand some of the simple calculations, the mass of solids, M_s, was measured at the end of the test, when a moisture content test was conducted in the sample after it was removed from the SWC cell. The following is a summary of the calculations used in the analysis,

1) The mass of water per mm change in the water tubes was calculated using the density-volume relationship of water at 20 ℃, where water density is about 0.001 g/mm^3.
2) At the end of the saturation phase, the total volume of the saturated sample, V_{sat}, was calculated using $V_{sat} = V_{ring} + V_{exp}$, where V_{exp} is the volume change due to the expansion, which is the elevation increase multiplied by the surface area of the ring.
3) The void ratio at the end of the saturation phase was calculated using specific gravity, G_s, water density, ρ_w, and dry density, $\rho_d = \frac{M_s}{V_{sat}}$

$$e = \frac{G_s \times \rho_w}{\rho_d} - 1 \qquad (3-6)$$

4) New specimen thickness, b, was calculated after subtracting the measured elevation change.
5) Assuming uniform linear change in diameter due to shrinkage after applying suction, interpolation was used to calculate the diameter correspond to each suction value, d_{est}, using the initial diameter, diameter of the ring, at 0 suction and the final diameter, measured at the end of the test, which is corresponded to 1400 kPa of suction.
6) Change in volume was divided into two steps
    a. Due to elevation change, ΔV_{elev}, and calculated as

$$\Delta V_{elev} = A_{ring} \times \Delta h \qquad (3-7)$$

7) Where, A_{ring} is the area of the brass ring in mm^2 and Δh is the measured elevation change
    a. Laterally due to shrinkage, ΔV_{shrink}, and calculated as

$$\Delta V_{shrink} = \frac{\pi}{4}\left(d_{ring}^2 - d_{est}^2\right) \times b \qquad (3-8)$$

8) Calculating the new volume, V, was simply done by subtracting the cumulative change in volume from the original volume, V_{sat}.
9) Then, subsequent dry density and void ratio were calculated, same as step 3, and strain was calculated as

$$\varepsilon = \frac{\Delta e}{1 + e_0} \qquad (3-9)$$

10) Where e_0 is always the void ratio calculated at the end of the saturation phase
11) The mass of water at saturation, $M_{w_{sat}}$, and at the end of the test, $M_{w_{end}}$, after applying 1400 kPa of suction, were calculated. Also, the mass of remained water inside the sample at the end of testing was estimated based on the cumulative of released water measurements, $M_{w_{est}}$. The difference between the $M_{w_{end}}$ and $M_{w_{est}}$ was used as a correction factor to the measured mass of water.
12) Moisture content, $\boldsymbol{\omega}$, was calculated using the corrected measured mass of water, $M_{w_{corrected}}$, and M_s.
13) The Degree of Saturation, S (%), was calculated using:

$$S(\%) = \frac{\omega G_s}{e} \times 100 \qquad (3-10)$$

14) It was assumed that the samples remained fully saturation at the end of the consolidation phase, before applying any suction. Thus, values were normalized to start from S (%) = 100.

3.9. Results

The results are summarized based on the parameters, void ratio, strain, moisture content, and degree of saturation, in Table 3.4 through Table 3.15. Each parameter contains three 3-D models for *w*PI equals a) 10, b) 30, and 3) 50, Figure 3.8 through Figure 3.11, representing the change in the parameter due to the change in suction ($\Delta\Psi$) and the change in net normal stresses ($\Delta\sigma$).

Table 3.4 Void Ratio, e, Values for Category 1, *w*PI =10

Test	Net Normal Stress (kPa)	Suction (kPa)				
		0	100	500	1000	1400
1	1	0.662	0.659	0.645	0.629	0.616
2	10	0.679	0.666	0.652	0.635	0.621
3	20	0.662	0.652	0.629	0.609	0.594
4	40	0.661	0.653	0.629	0.610	0.599
5	60	0.554	0.547	0.526	0.517	0.513

Table 3.5 Void Ratio, e, Values for Category 2, *w*PI =30

Test	Net Normal Stress (kPa)	Suction (kPa)				
		0	100	500	1000	1400
1	1	0.822	0.817	0.797	0.771	0.751
2	10	0.835	0.810	0.760	0.719	0.691
3	20	0.830	0.805	0.751	0.710	0.682
4	40	0.751	0.726	0.700	0.668	0.644
5	60	0.677	0.664	0.638	0.619	0.606

Table 3.6 Void Ratio, e, Values for Category 3, *w*PI =50

Test	Net Normal Stress (kPa)	Suction (kPa)				
		0	100	500	1000	1400
1	1	1.061	1.040	1.026	0.993	0.966
2	10	1.053	1.013	0.961	0.931	0.907
3	20	1.051	1.015	0.947	0.903	0.873
4	40	0.961	0.917	0.858	0.810	0.776
5	60	0.745	0.701	0.610	0.563	0.532

Table 3.7 Strain, ε, Values for Category 1, *w*PI =10

Test	Net Normal Stress (kPa)	Suction (kPa)				
		0	100	500	1000	1400
1	1	0	0.008	0.012	0.02	0.027
2	10	0.001	0.009	0.017	0.027	0.035
3	20	0.003	0.009	0.023	0.035	0.043
4	40	0.006	0.011	0.025	0.036	0.043
5	60	0.077	0.081	0.093	0.099	0.101

Table 3.8 Strain, ε, Values for Category 2, *w*PI =30

Test	Net Normal Stress (kPa)	Suction (kPa)				
		0	100	500	1000	1400
1	1	0.000	0.003	0.014	0.028	0.039
2	10	0.004	0.017	0.045	0.067	0.082
3	20	0.008	0.022	0.051	0.073	0.088
4	40	0.036	0.050	0.064	0.082	0.095
5	60	0.088	0.095	0.109	0.120	0.127

Table 3.9 Strain, ε, Values for Category 3, *w*PI =50

Test	Net Normal Stress (kPa)	Suction (kPa)				
		0	100	500	1000	1400
1	1	0.000	0.010	0.017	0.033	0.046
2	10	0.007	0.026	0.052	0.066	0.077
3	20	0.007	0.024	0.057	0.078	0.093
4	40	0.067	0.088	0.116	0.139	0.155
5	60	0.176	0.197	0.240	0.262	0.277

Table 3.10 Moisture Content, ω (%), Values for Category 1, *w*PI =10

Test	Net Normal Stress (kPa)	Suction (kPa)				
		0	100	500	1000	1400
1	1	22	17	14	13	12
2	10	22	17	15	13	12
3	20	21	17	15	13	12
4	40	20	17	15	12	12
5	60	21	19	16	14	12

Table 3.11 Moisture Content, ω (%), Values for Category 2, *w*PI =30

Test	Net Normal Stress (kPa)	Suction (kPa)				
		0	100	500	1000	1400
1	1	28	24	21	19	17
2	10	30	25	22	19	19
3	20	29	22	19	18	17
4	40	28	23	20	18	17
5	60	26	22	21	19	18

Table 3.12 Moisture Content, ω (%), for Category 3, *w*PI =50

Test	Net Normal Stress (kPa)	Suction (kPa)				
		0	100	500	1000	1400
1	1	37	31	28	25	24
2	10	37	32	29	28	26
3	20	38	32	28	26	24
4	40	39	31	28	26	24
5	60	40	33	29	27	24

Table 3.13 Degree of Saturation, S (%), Values for Category 1, *w*PI =10

Test	Net Normal Stress (kPa)	Suction (kPa)				
		0	100	500	1000	1400
1	1	100	80	69	63	60
2	10	100	80	72	66	62
3	20	100	88	81	73	70
4	40	100	87	81	73	71
5	60	100	95	83	73	70

Table 3.14 Degree of Saturation, S (%), Values for Category 2, *w*PI =30

Test	Net Normal Stress (kPa)	Suction (kPa)				
		0	100	500	1000	1400
1	1	100	86	79	75	70
2	10	100	86	80	76	78
3	20	100	80	75	73	74
4	40	100	85	75	72	71
5	60	100	86	83	76	76

Table 3.15 Degree of Saturation, S (%), Values for Category 3, *w*PI =50

Test	Net Normal Stress (kPa)	Suction (kPa)				
		0	100	500	1000	1400
1	1	100	87	79	75	72
2	10	100	90	86	86	82
3	20	100	87	82	80	78
4	40	100	81	76	74	72
5	60	100	82	84	82	74

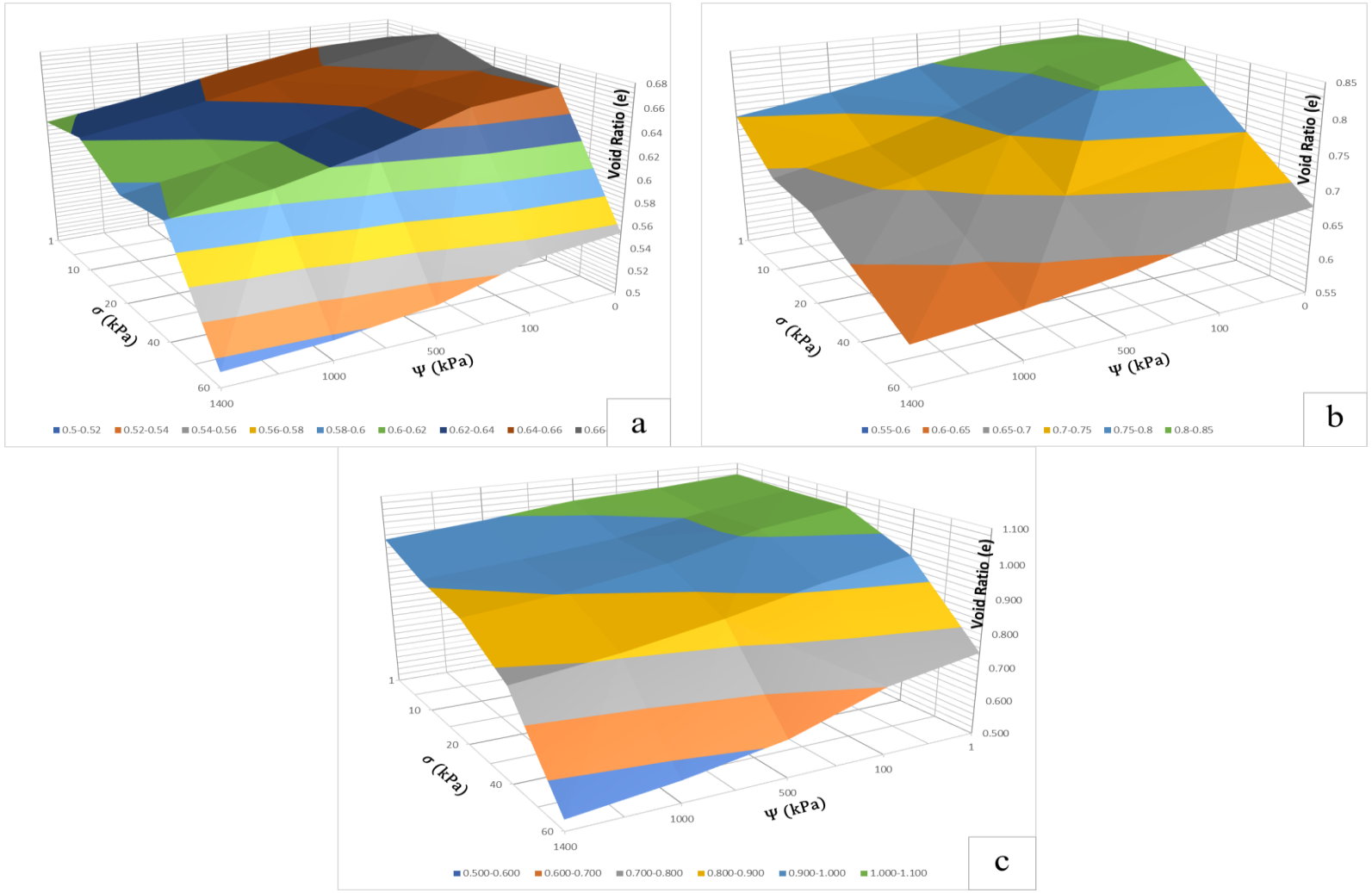

Figure 3.8 Void Ratio Results for Soil with *wPI* Equals a) 10, b) 30, and c) 50

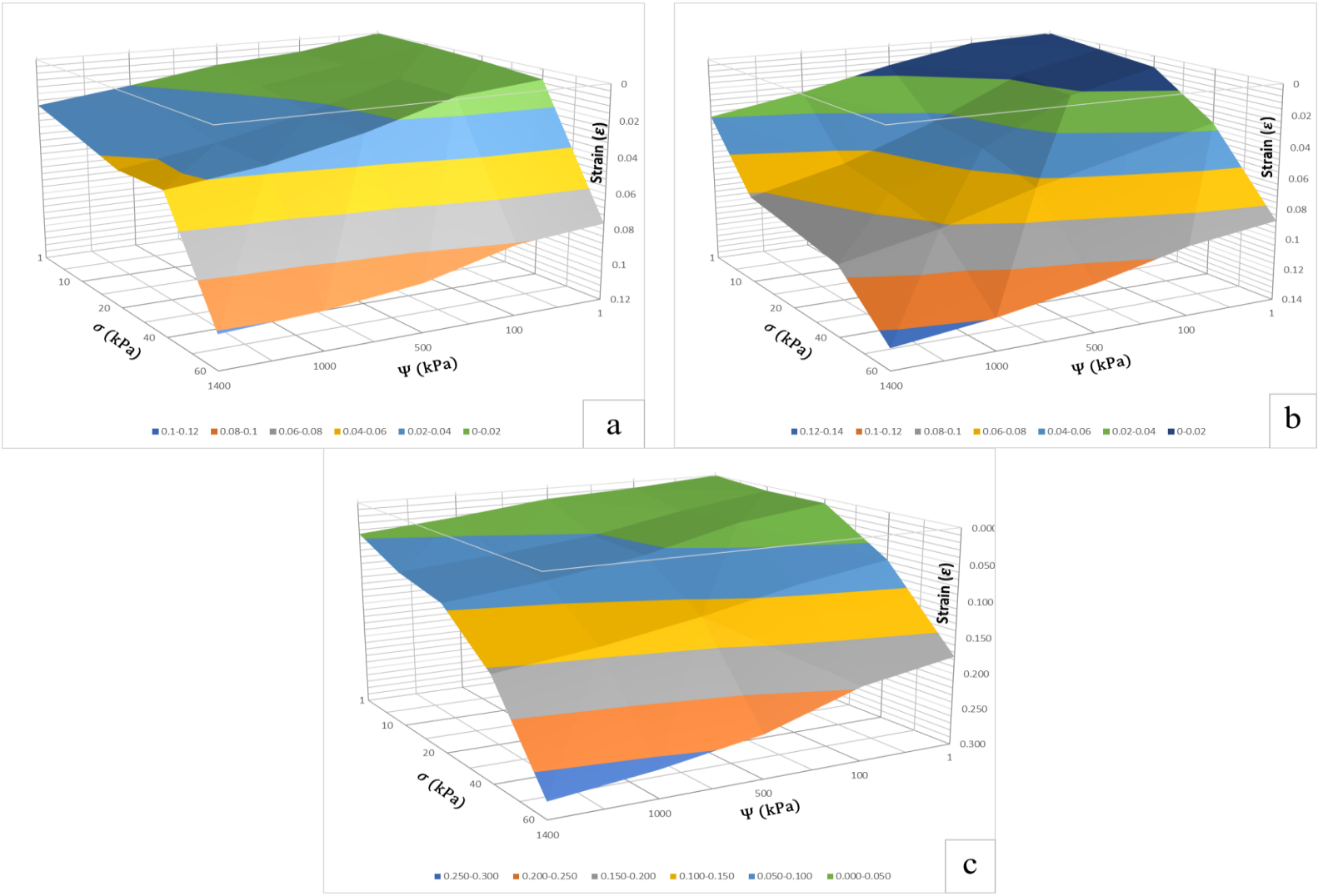

Figure 3.9 Strain Results for Soil with *w*PI Equals a) 10, b) 30, and c) 50

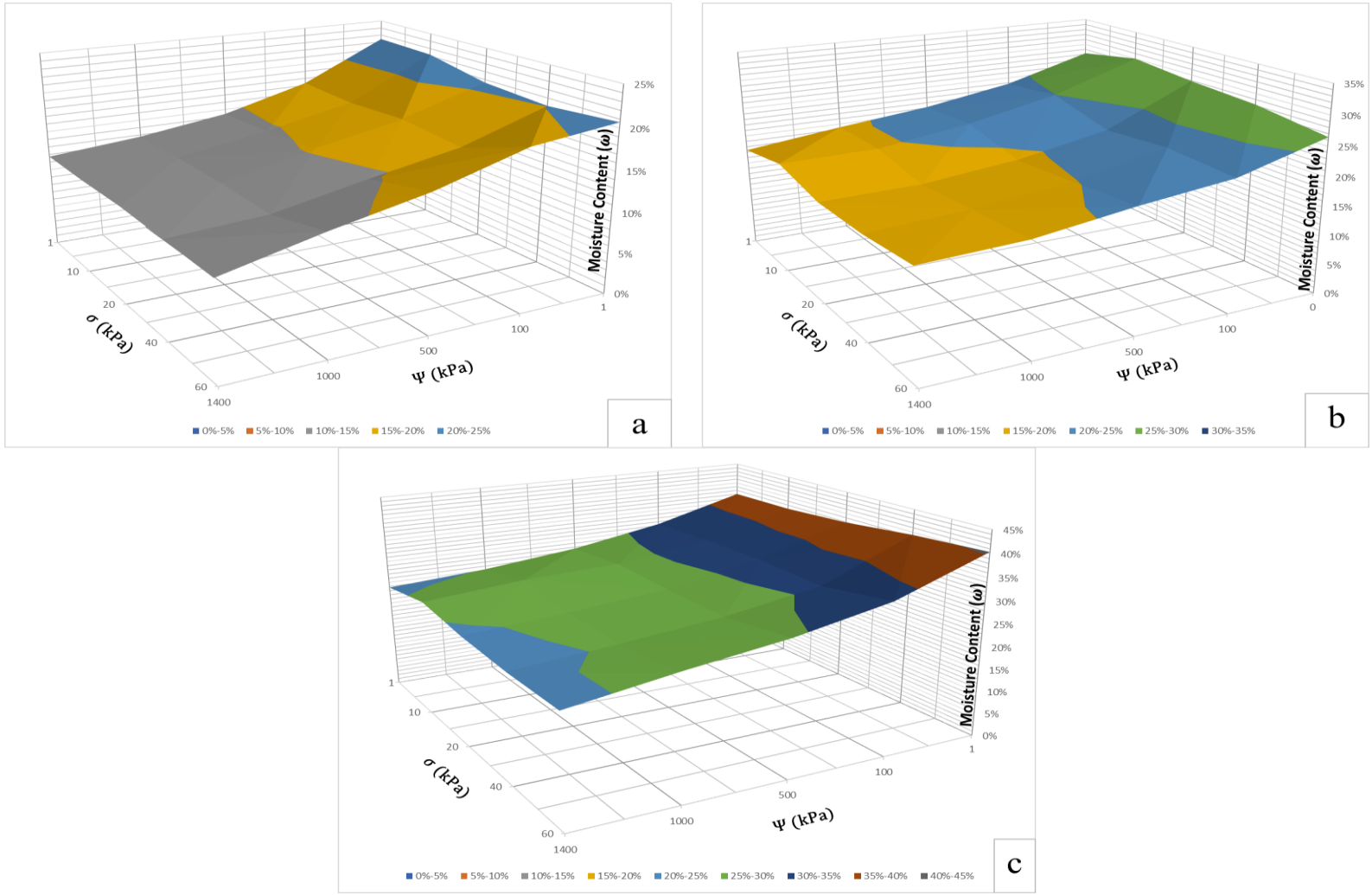

Figure 3.10 Gravimetric Moisture Content Results for Soil with *w*PI Equals a) 10, b) 30, and c) 50

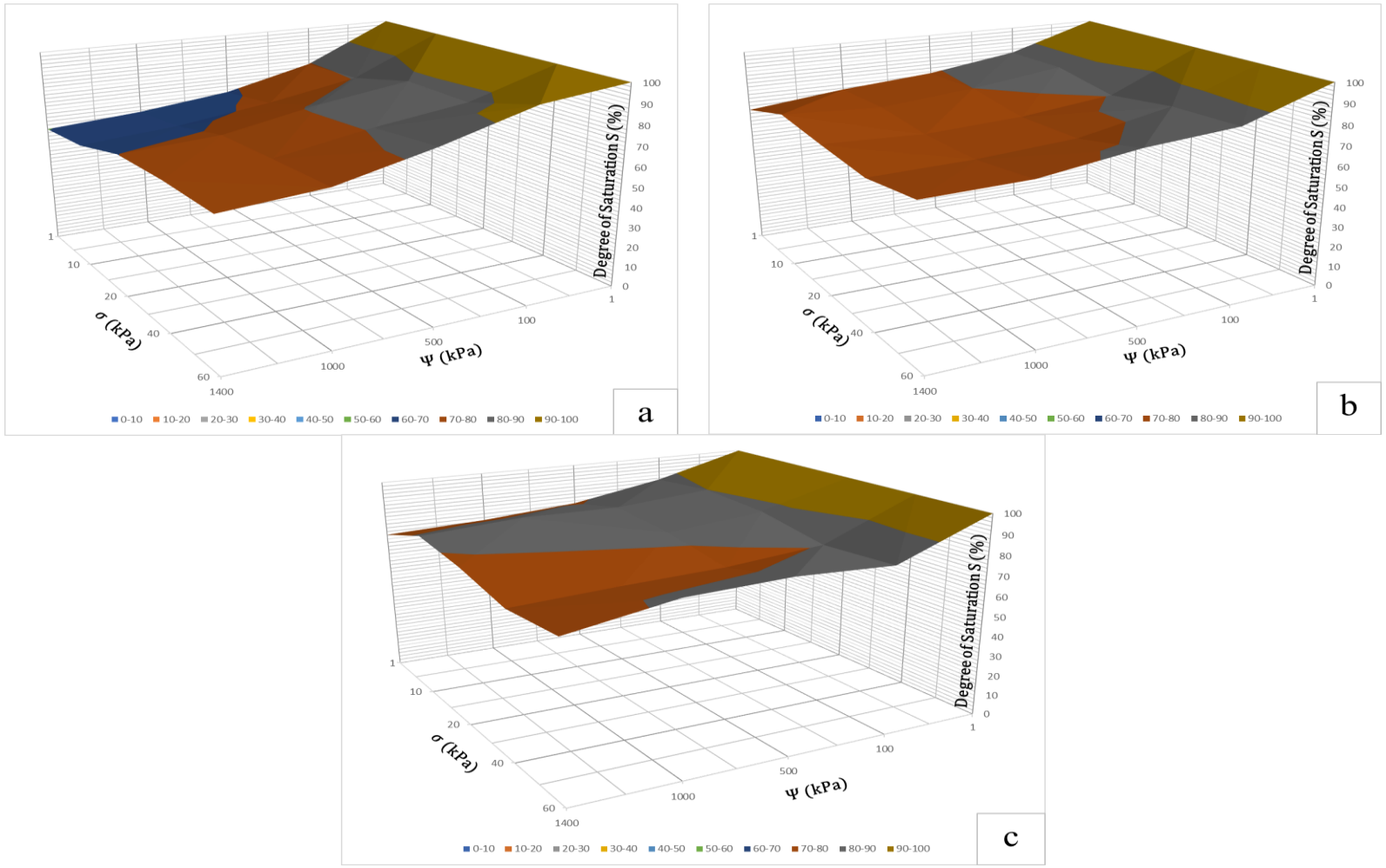

Figure 3.11 Degree of Saturation Results for Soil with *w*PI Equals a) 10, b) 30, and c) 50

3.10. Discussion

3.10.1. Troubleshooting

Although troubleshooting had minor effects on the results, the discussion is presented as it affected the overall duration of this laboratory testing.

- Some details in the procedure were changed during testing.
    - Step 3 in the procedure section was not done originally as explained. The change in height due to expansion during the saturation phase was not measured for six of the specimens used.
        - No measurements were taken for the specimens used in category two but the one with lowest net normal stress. The value found for this specimen is assumed for the non-measured ones.
        - No measurements were taken for two of the specimens with highest net normal stresses used in category 4. Therefore, the value measured for the second specimen was used for both. For more detailed information, please refer to Appendix C.
    - For the fourth sample of the category 1, the degree of saturation at the end of the test was expectedly irrational since some of the water evaporated and corrections were made trying to cover the loss of water by adding only the lost amount. Based on the results, the corrections were not enough, and it is believed that unmeasured amount of water was also lost. As a result, the S (%) value at Ψ = 1400 kPa and σ_n= 60 kPa was corrected from 60% to 70%.
- It was found that during the consolidation phase, since no suction was applied, water was entering the chamber, originally considered as water absorbed by the specimen, and hanging on top of the porous stone. As a result, the water absorbed was not considered in the calculations because no evidence was found that the amount of water that entered the chamber during the consolidation phase was, in fact, absorbed by the specimen. This is the reason steps 11 and 12 in the calculations section were added.
- The main problem one may face is water and/or air leakage. Leakage was difficult to detect and sometimes appeared only at higher suction levels. Some results showed negative water change found, which means absorption, during the higher suction, which was not expected. As a result, correction factors were used to replace the amount of lost water, step 13 in the calculations section. To correct this troubleshooting, step 7 in the procedure section was added.

3.10.2. Analysis

3.10.2.1 Sensitivity Analysis Results

Three dimensional relationships of the change in suction ($\Delta\Psi$), the change in net normal stress ($\Delta\sigma$), and measured and/or calculated void ratio, e, strain, $\boldsymbol{\varepsilon}$, moisture content, $\boldsymbol{\omega}$, or degree of saturation, S, were developed to find the best correlation to estimate volume change. The variables, *w*PI, $\Delta\Psi$, and $\Delta\sigma$ were the three independent variables considered in the analysis.

- In general, void ratio decreased as the $\Delta\Psi$ or $\Delta\sigma$ increased as it appears in Figure 3.8. Figure 3.9 shows that strain, on the other hand, increased by increasing $\Delta\Psi$ or $\Delta\sigma$. Those results are in accordance with reporting literature.
- Regardless of the change in net normal stress, moisture content maintained approximately constant values under a constant suction. However, increasing *w*PI increased the moisture content as it appears in Table 3.10. through Table 3.12.
- The degree of saturation, which is a function of $\boldsymbol{\omega}$ and e, generally decreased as Ψ increased, at a constant net normal stress. Only 5 points out of the 75 points measured did not follow the expected trend. However, increasing σ and/or *w*PI results in relatively random relationship between degree of saturation and suction as it appears in Figure 3.11. The reason is that as the $\boldsymbol{\omega}$ decreases by increasing suction, e is also decreasing due to the increase in σ. Because the effects of $\boldsymbol{\omega}$ and e on S are opposite, S increased or decreased as σ increased depending on the amount of change in e compared to the change in $\boldsymbol{\omega}$.

An additional sensitivity analysis was conducted through two dimensional relationships for each parameter for further observations. Appendix F contains all developed 2-D charts. In the following, a summary of observations is presented based on the charts in Figure 3.12 through Figure 3.15.

1. σ (in log scale) at *w*PI = 50 for different Ψ values shown in Figure 3.12
    a) This chart is the typical e versus log σ plot from which preconsolidation pressure (P_p) and compression index (C_c), or coefficient of compressibility (a_t) used in the net normal stress slope as mentioned in Figure 3.4, can be determined.
    b) Strain increased as σ increased following a similar path as the void ratio.
    c) Moisture content decreased as Ψ increased, but approximately maintained a constant value as σ increased.
    d) The degree of saturation showed a random relationship by increasing at the beginning and at the end while decreasing in the middle as σ increased.
2. Ψ (in log scale) at *w*PI = 50 for different σ values shown in Figure 3.13
    a) The slope in this chart is the coefficient of compressibility (a_m) used in the matric suction slope as mentioned in Figure 3.4.
    b) When compared to the charts for both void ratio and strain in Figure 3.12, the effect of σ alone is more than 3 times the effect of Ψ. Also, the change due to the coupled stresses, Ψ and σ, is about 28% higher than the summation of the changes due to each stress individually. Note that this only applies to the *w*PI = 50 soils. For the other soils, very small difference was found, 3% and less.
    c) For moisture content chart, this is the soil water characteristic curve (SWCC), and the slope is b_m as mentioned in Figure 3.5.
    d) This is another form of SWCC using the degree of saturation.
3. Ψ (in log scale) at σ = 60 kPa for different *w*PI values shown in Figure 3.14
    a) Due to suction increase, the change in void ratio increased for *w*PI of 50 and *w*PI of 30 compared to the *w*PI of 10 by about 415% and 72% respectively.
    b) Due to suction increase, the change in strain increased for *w*PI of 50 and *w*PI of 30 compared to the *w*PI of 10 by about 359% and 45% respectively.

c) Due to suction increase, the reduction in moisture content for *w*PI of 30 is almost equals to the reduction in $\boldsymbol{\omega}$ for the *w*PI of 10. However, the reduction in $\boldsymbol{\omega}$ for the *w*PI of 50 is almost doubled.

d) The degree of saturation reached minimum values of 70%, 76%, and 74% for soil of *w*PI of 10, *w*PI of 30, and *w*PI of 50, respectively.

4. *w*PI at Ψ = 1400 kPa for different σ values shown in Figure 3.15

a) Much higher compressibility was observed for the most expansive soil. The change in e increased for *w*PI of 50 and *w*PI of 30 compared to the *w*PI of 10 by about 399% and 32% respectively.

b) Similarly, the change in $\boldsymbol{\varepsilon}$ increased for *w*PI of 50 and *w*PI of 30 compared to the *w*PI of 10 by about 269% and 27% respectively.

c) The moisture content tried to maintain a constant value regardless the increase in σ. The average $\boldsymbol{\omega}$ is 12%, 17.5%, and 24.5% for *w*PI of 10, *w*PI of 30, and *w*PI of 50, respectively.

d) Degree of saturation increased as *w*PI increased for σ = 1, 10, and 20. For σ = 40, S remained almost constant. For σ = 60, S increased from *w*PI of 10 to *w*PI of 30 but then decreased from *w*PI of 30 to *w*PI of 50

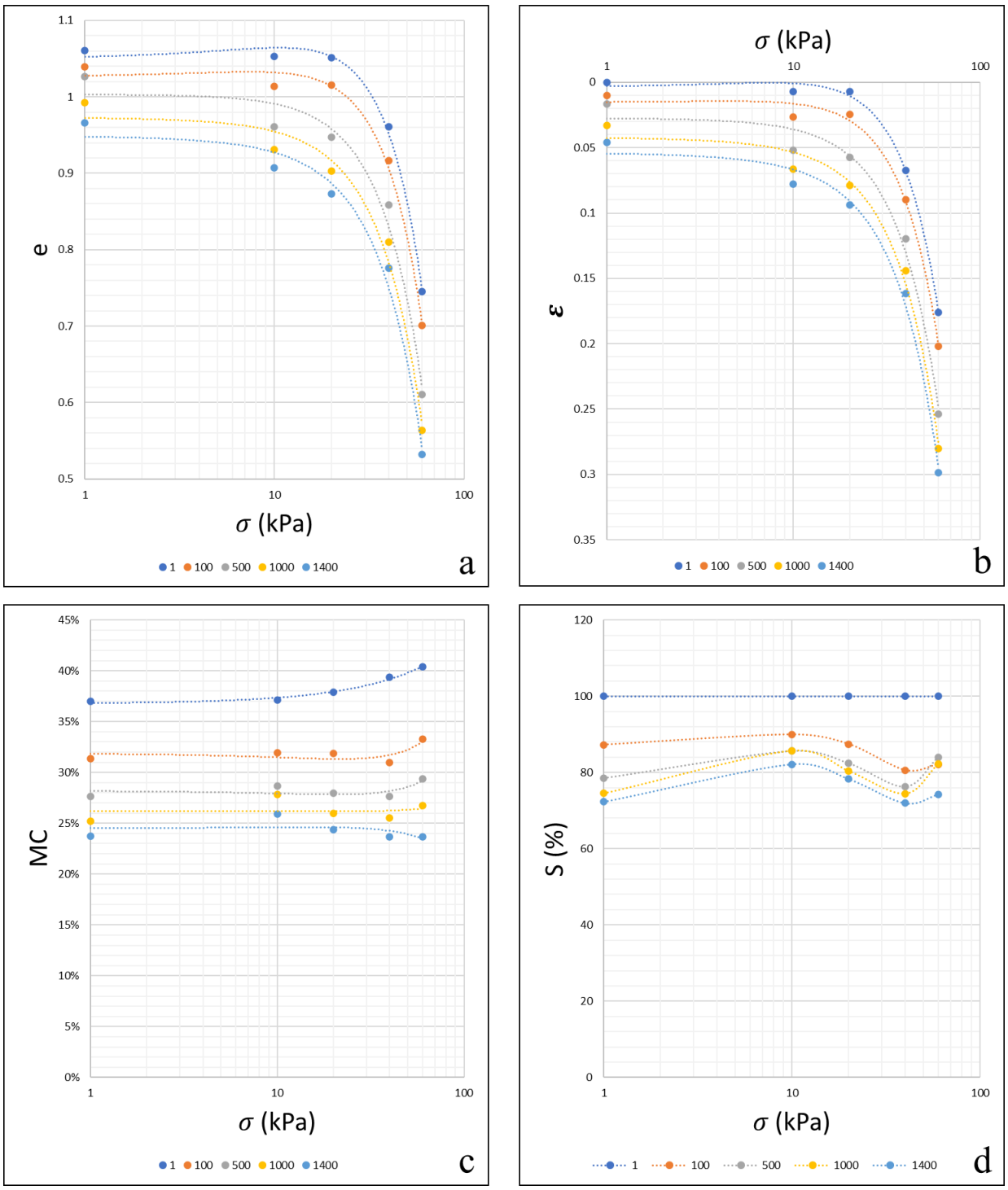

Figure 3.12 a) Void Ratio, b) Strain, c) Moisture Content, and d) Degree of Saturation as a Function of σ (in Log Scale) at *w*PI = 50 for Different Ψ Values

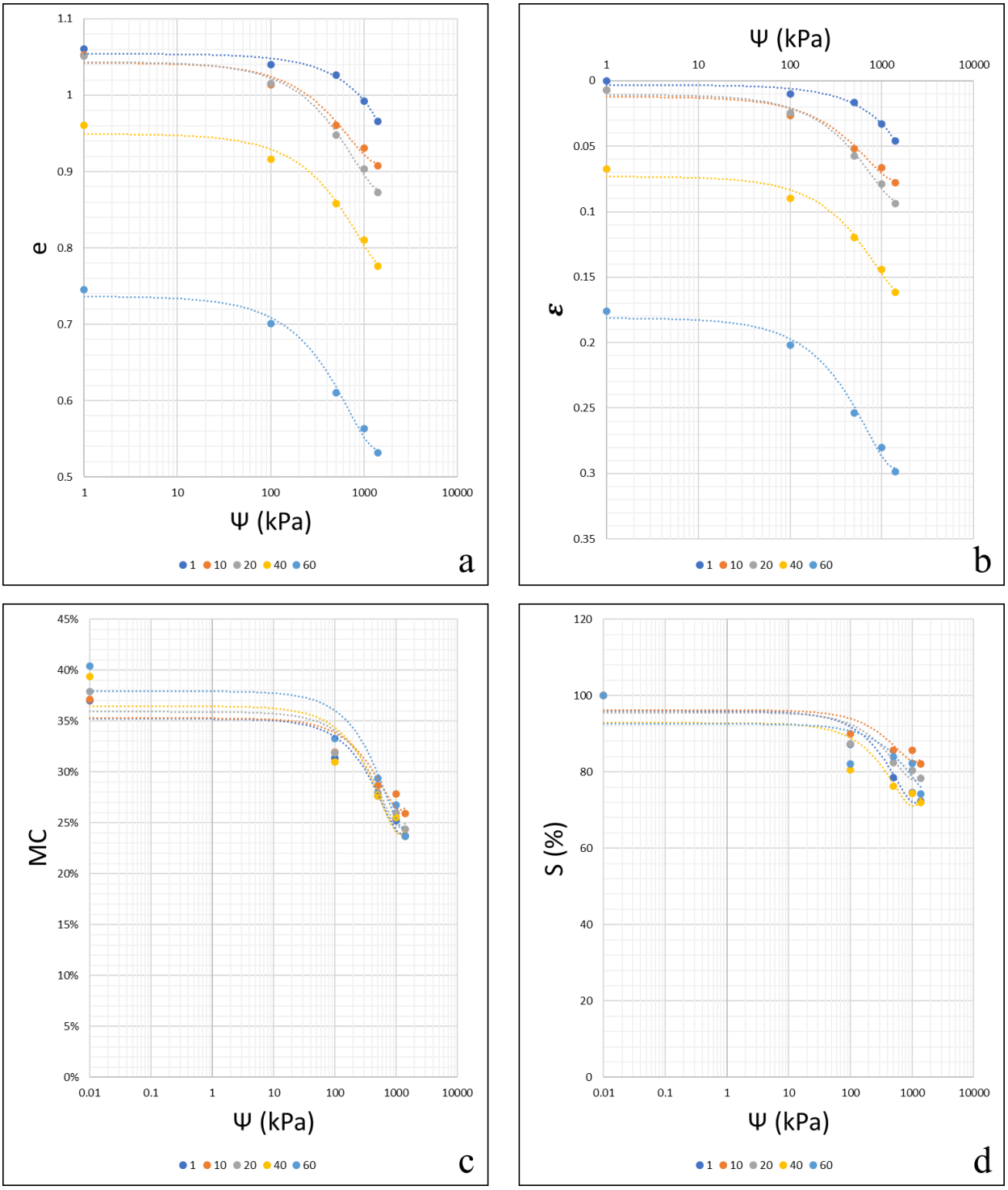

Figure 3.13 a) Void Ratio, b) Strain, c) Moisture Content, and d) Degree of Saturation as a Function of Ψ (in Log Scale) at *w*PI = 50 for Different σ Values

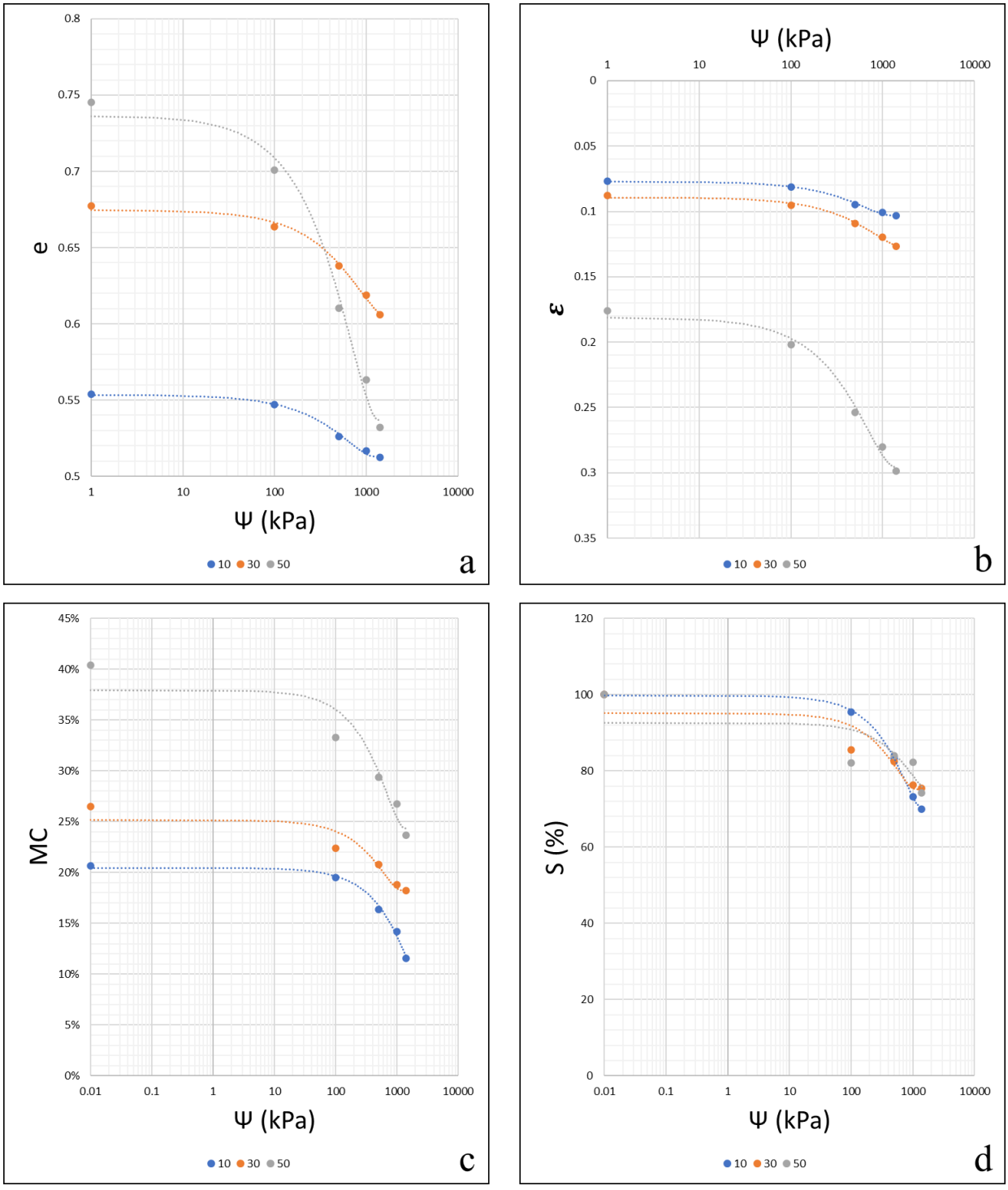

Figure 3.14 a) Void Ratio, b) Strain, c) Moisture Content, and d) Degree of Saturation as a Function of Ψ (in Log Scale) at σ = 60 for Different *w*PI Values

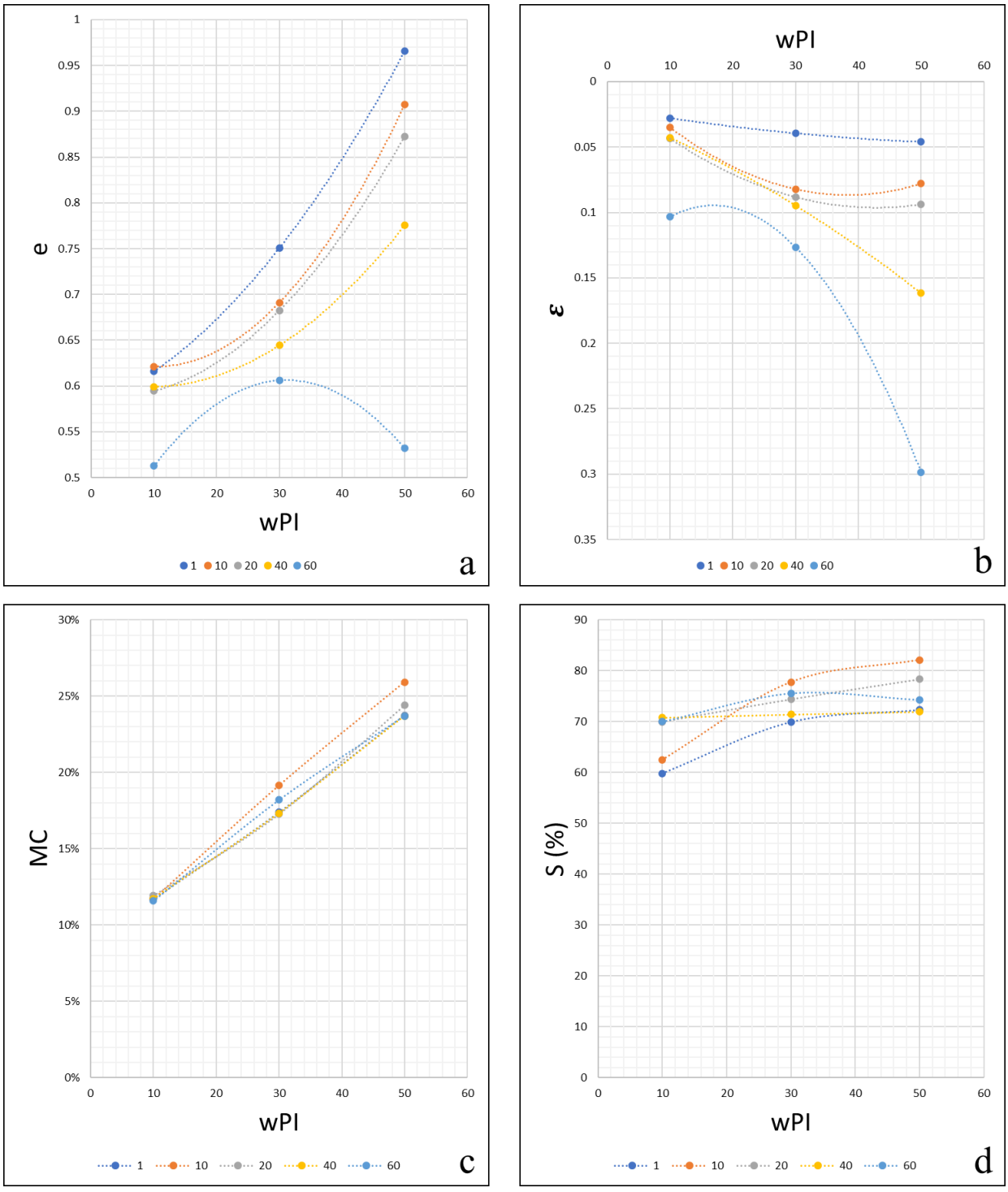

Figure 3.15 a) Void Ratio, b) Strain, c) Moisture Content, and d) Degree of Saturation as a Function of *w*PI for Different σ Values

3.10.2.2 Statistical Analysis

Since the overall results of both void ratio and strain can be considered logical, statistical analysis was conducted to figure the best empirical relationship to estimate volume change due to the soil type, using *w*PI, and the coupled stresses, suction and net normal. Different parameters, such as square, log, etc., were used for each independent to find the best correlation. For both e and $\boldsymbol{\varepsilon}$, simple linear correlation of *w*PI, Ψ, and σ was found to have the best fit regression. The results for both can be found in Table 3.16.

Table 3.16 The Results of The Statistical Analysis for e and $\boldsymbol{\varepsilon}$.

Parameter		Coefficients	P-value	R^2
Void ratio (e)	Intercept	0.677310	1.72E-49	0.86
	*w*PI	0.006796	1.05E-26	
	Ψ (kPa)	-7.44E-05	5.73E-08	
	σ (kPa)	-0.003493	1.13E-17	
Strain ($\boldsymbol{\varepsilon}$)	Intercept	-0.062724	9.86E-09	0.77
	*w*PI	0.001550	1.14E-09	
	Ψ (kPa)	4.03E-05	9.68E-08	
	σ (kPa)	0.002056	5.67E-19	

As presented in Table 3.16, void ratio is showing a higher R^2 value. As a quick sensitivity analysis check, the *w*PI coefficient is positive, which means that when Ψ and σ are close to zero, the e increases by increasing *w*PI. On the other hand, the coefficients of Ψ and σ are both negative, which means as one or both increases, the e decreases. Similar relationship was expected and found in this study.

Strain, on the other hand, starts from a negative value, the intercept, and increases as any of the independents increases, since all have positive coefficients. This relationship matches the results. However, the strain was always calculated from complete saturation, i.e., after reaching maximum expansion, so no negative strain value can be found in the analysis. Yet, if *w*PI of 10 is used with zero Ψ and σ strain will be negative, which does not match the results. This can be considered a statistical relationship error and may be negligible. Still, the void ratio analysis showed better correlation.

As a result, the following void ratio, e, equation was found to be the best correlated empirical equation to estimate volume change due to expansive soil behavior.

$$\Delta e = 0.67731 + 0.006796\ (w\text{PI}) - 7.44 \times 10^{-5}(\Delta\Psi) - 0.003493\ (\Delta\sigma) \qquad (3-11)$$

3.11. Conclusion

Laboratory research work performed to estimate the volume change of compacted specimens due to the application of coupled net normal and suction stresses was conducted. The results were used to propose a model to estimate volume change of soils of a wide range of expansion potential.

A 1-D oedometer-type pressure plate device (SWC-150) was used for the laboratory testing. This device can apply net normal stress while following various applied matric suctions. Volume changes due to both stresses were measured and/or calculated in a coupled procedure. The suction compression index was

measured under drying conditions and an empirical relationship between changes of void ratio, matric suction, net normal stress, and *w*PI was developed. The results of this study greatly enhance the prediction of strains due to suction changes and allow for the evaluation of the couple effects when the net normal stresses are simultaneously acting on the soil material.

Both void ratio (e) and strain ($\boldsymbol{\varepsilon}$) showed rational relationship with change in *w*PI, suction (Ψ), and net normal stress (σ). Statistical analysis was conducted for both e and $\boldsymbol{\varepsilon}$. The best correlated empirical equation to estimate volume change affected by *w*PI, Ψ, and σ was found using e with R^2 of 86%.

3.12. References

ASTM D4546. (2014). *Standard Test Method for One-Dimensional Swell or Settlement Potential of Cohesive Soils*.

ASTM D 854-02. Standard Test Methods for Specific Gravity of Soil Solids by Water Pycnometer.

Chen, P., and Lu, N. (2018). *Generalized Equation for Soil Shrinkage Curve.* Journal of Geotechnical and Geoenvironmental Engineering, vol. 144, no. 8, 2018, p. 04018046., https://doi.org/10.1061/(asce)gt.1943-5606.0001889.

Fredlund, D. G., Rahardjo, H., and Fredlund, M.D. (2012). *Unsaturated Soil Mechanics in Engineering Practice.* Wiley.

Fredlund, D., Morgenstern, N. (1977). *Stress State Variables for Unsaturated Soils.* Journal of the Geotechnical Engineering Division, 103(G75), 441-466.

Fredlund, D., and Rahardjo, H. (1993). *Soil Mechanics for Unsaturated Soils.* Wiley Inter-Science

GCTS Testing Systems. (2007). SWC-150: *Fredlund Soil Water Characteristic Device. 1.3.* Tempe, AZ.

Holtz, R. D., & Kovacs, W. (1981). *Engineering Properties of Expansive Clays*. ASCE, 121, 641-677.

Houston, S., & Houston, W. (2017). Suction-Oedometer Method for Computation of Heave and Remaining Heave. 2nd Pan-American Conference on Unsaturated Soils. Dallas, TX: ASCE.

Lytton, R. L. (1977). *Foundations in Expansive Soils, in Numerical Methods in Geotechnical Engineering*, Chapter 13. (pp. 427-458). C. S. Desai & J. T. Christian (Eds.), New York: McGraw-Hill.

Lytton, R., Aubeny, C., and Bulut, R. (2005). *Design Procedures for Soils on Expansive Soils: Volume 1*. FHWA/TX-05/0-4518. Texas Department of Transportation.

McKeen, R. G. and Hamberg, D. J. (1981). *Characterization of Expansive Soils. Trans. Res. Rec. 790*, Trans. Res. Board, (pp. 73-78).

McKeen, R. G. and Johnson, L. D. (1990). *Climate-Controlled Soil Design Parameters for Mat Foundations.* J. of Geotechnical Eng., 116(7), 1073-1094.

Olaiz, Austin H. (2017). *Evaluation of Testing Methods for Suction-Volume Change of Natural Clay Soils.* Tempe, AZ: Arizona State University.

Pham, H. Q., and Fredlund, D. G. (2011). *Volume–Mass Unsaturated Soil Constitutive Model for Drying–Wetting under Isotropic Loading–Unloading Conditions.* Canadian Geotechnical Journal, vol. 48, no. 2, 2011, pp. 280–313., https://doi.org/10.1139/t10-061.

Post-Tensioning Institute. (2004). *Design of Post-Tensioned Slabs-on-Ground.* Phoenix: 3rd Edition, Post-Tensioning Institute.

Post-Tensioning Institute, (2008). *Design and construction of post-tensioned slabs-on-ground, 3rd edition.* Post Tensioning Institute, Phoenix.

Randy Rainwater, N, McDowell, L., Drumm, E. (2012). *Measurement of Total Soil Suction Using Filter Paper: Investigation of Common Filter Papers, Alternative Media, and Corresponding Confidence.* Geotechnical Testing Journal, vol. 35, no. 2, 2012, https://doi.org/10.1520/GTJ103204.

Singhal, S. (2010). *Expansive soil behavior: property measurement techniques and heave prediction methods.* Tempe, AZ: Arizona State University.

Singhal, S., Houston, S., & Houston W. (2011). *Effects of Testing Procedures on the laboratory Determination of Swell Pressure of Expansive Soils.* ASTM Geotechnical Testing Journal, 34, 476-488.

Sridharan, A, and P.V Sivapullaiah. (2005). *Mini Compaction Test Apparatus for Fine Grained Soils.* Geotechnical Testing Journal, Vol. 28, No. 3, pp. 240–246.

Texas Department of Transportation Material and Tests Division (1995). *"Determination of Potential Vertical Rise"*. Manual of Testing Procedures, Volume I. Test Method Tex-124-E.

Vann, J. D. (2019). *A Soil Suction-Oedometer Method and Design Soil Suction Profile Recommendations for Estimation of Volume Change of Expansive Soils.* Tempe, AZ: Arizona State University.

Vann, J.D., and Houston, S. (2021). *Field Suction Profiles for Expansive Soil*, J. of Geotechnical 746 and Geoenvironmental Engineering, 147(9), September 2021. 747 doi:10.1061/(ASCE)GT.1943-5606.0002570.

Vann, J., Houston, S., Houston, W., Singhar, S., Cuzme, A. and Olaiz, A. (2018). *A soil suction surrogate & its use in the suction-oedometer method for computation of volume change of expansive soils.* Proc. of the 7th International Conference on Unsaturated Soil. (pp 1205-1210). Hong Kong.

Zapata, C. E. (1999). *Uncertainty in Soil-Water-Characteristic Curve and Impacts on Unsaturated Shear Strength Predictions.* PhD Dissertation, Arizona State University.

Project No. 01-59

PROPOSED ENHANCEMENTS TO PAVEMENT ME DESIGN: IMPROVED CONSIDERATION OF THE INFLUENCE OF SUBGRADE SOILS SUSCEPTIBLE TO SHRINK/SWELL AND/OR FROST HEAVE ON PAVEMENT PERFORMANCE

APPENDIX 3A

TWO DIMENTIONAL RELATIONSHIP RESULTS FOR VOID RATIO, STRAIN, MOISTURE CONTENT, AND DEGREE OF SATURATION BASED ON WEIGHTED PLASITICITY INDEX, SUCTION, AND NET NORMAL STRESS

MAY 2023

LIST OF FIGURES

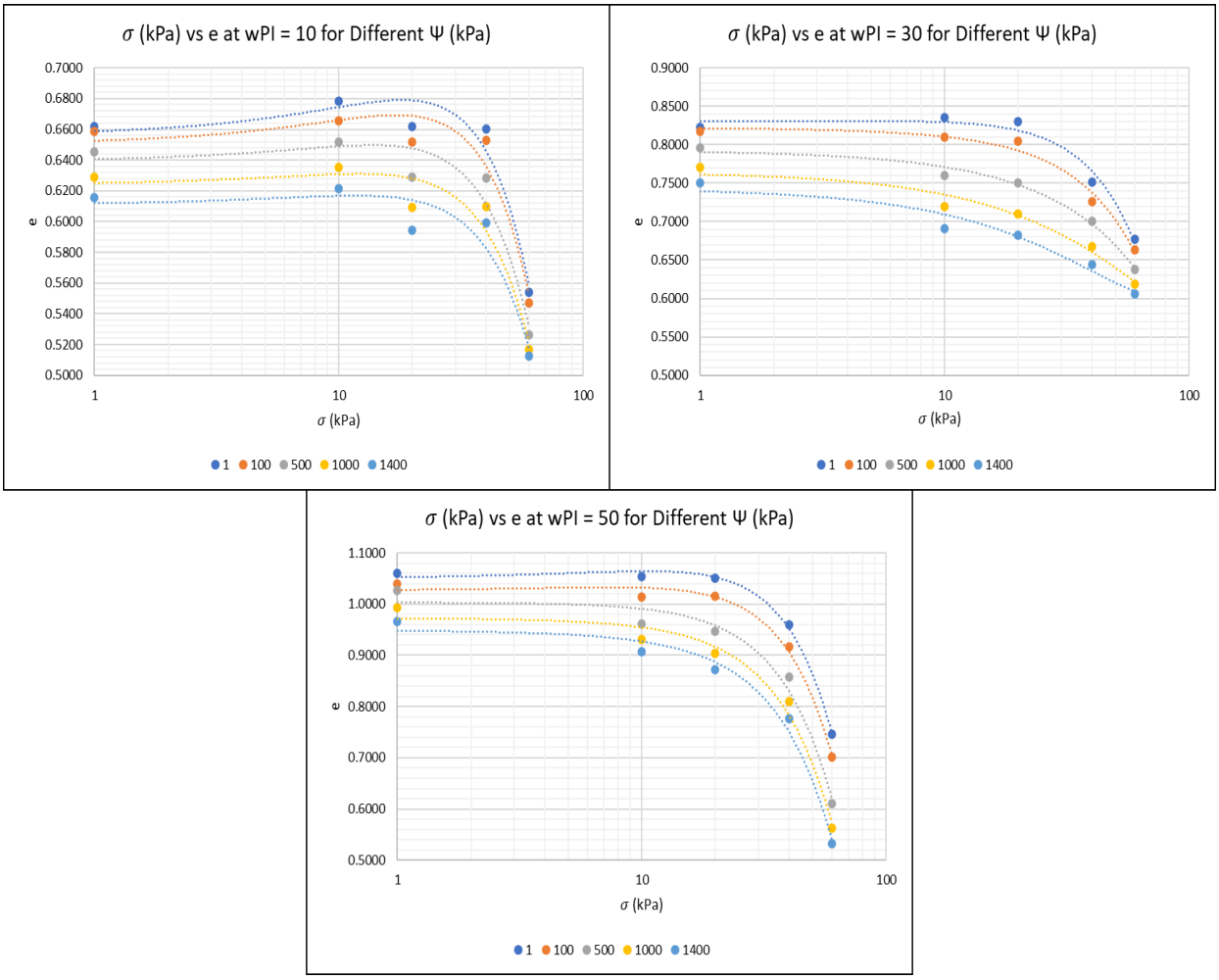

Figure 3A.1 Change in Void Ratio with Respect to Change in Net Normal Stress for Suction Values 1, 100, 500, 1000, and 1400

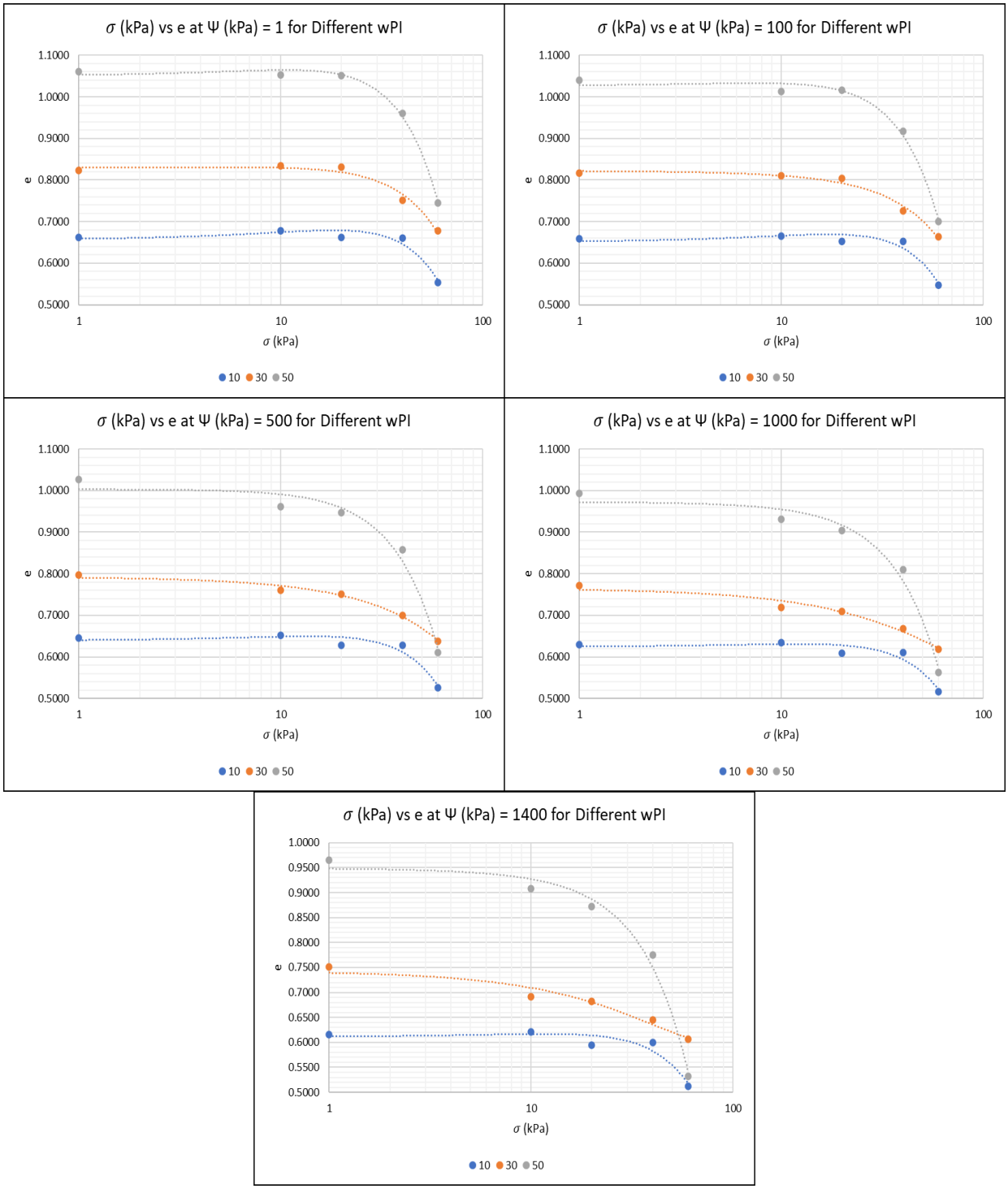

Figure 3A.2 Change in Void Ratio with Respect to Change in Net Normal Stress for *w*PI Values 10, 30, and 50

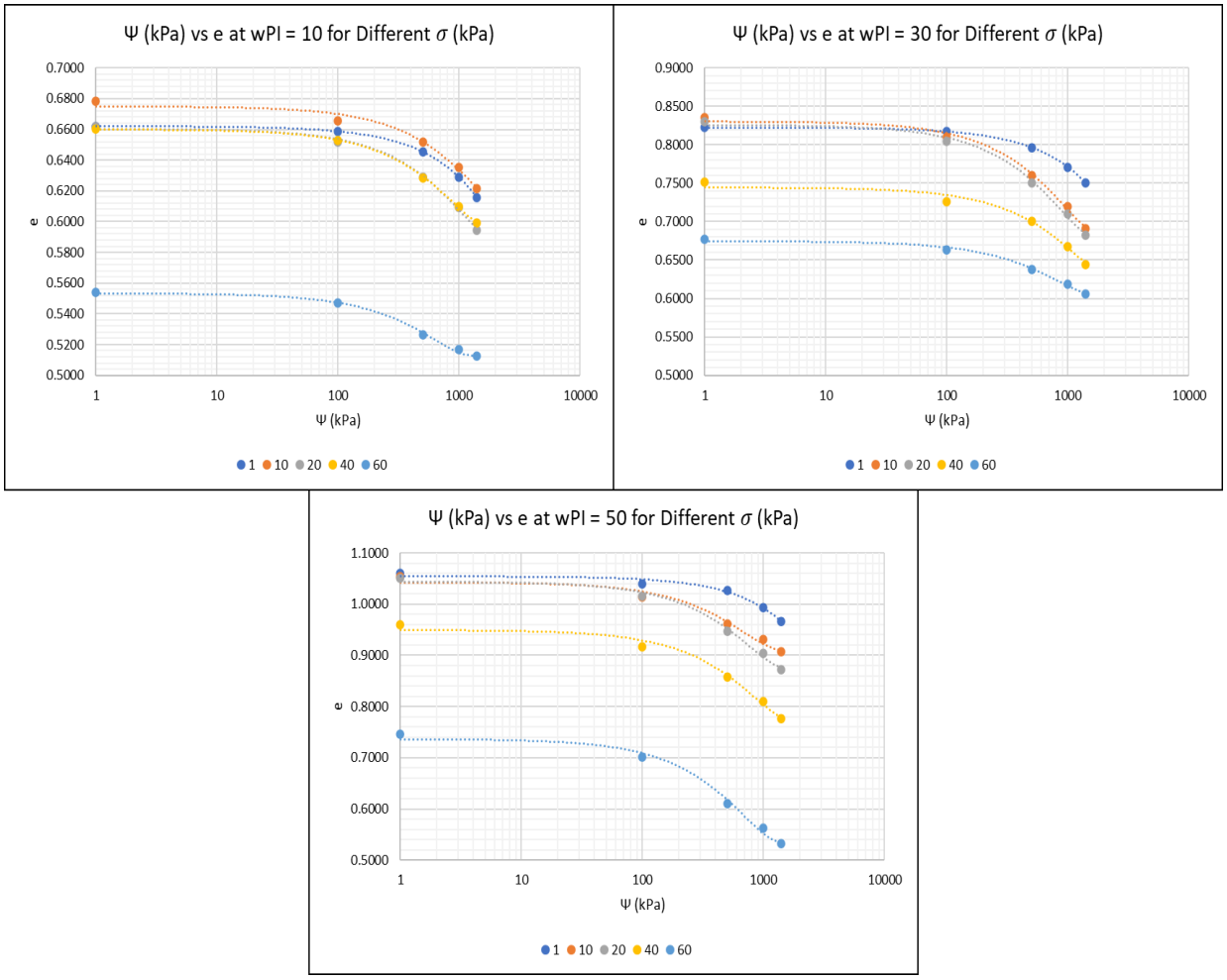

Figure 3A.3 Change in Void Ratio with Respect to Change in Suction for Net Normal Stress Values 1, 10, 20, 40, and 60

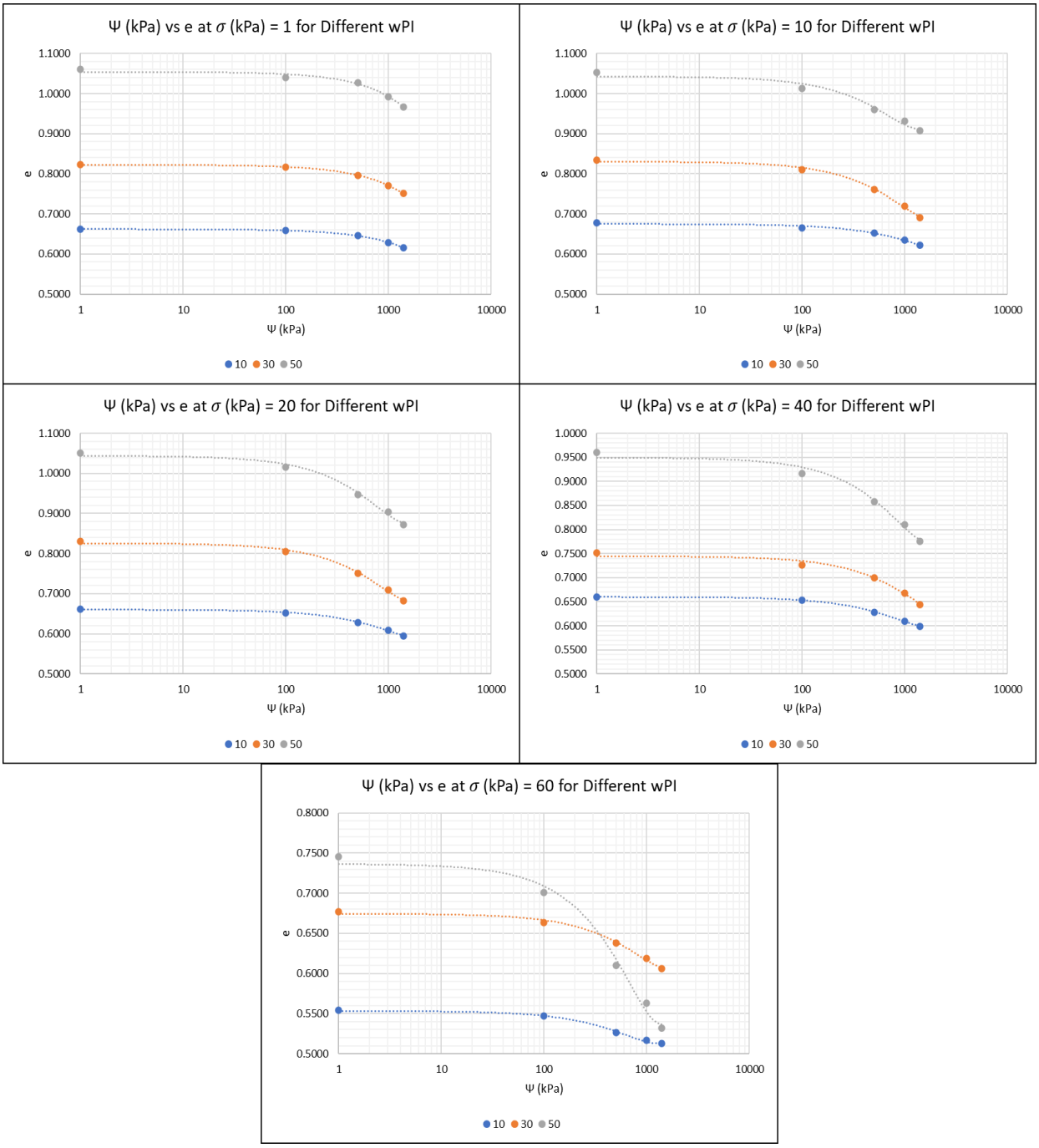

Figure 3A.4 Change in Void Ratio with Respect to Change in Suction for *w*PI Values 10, 30, and 50

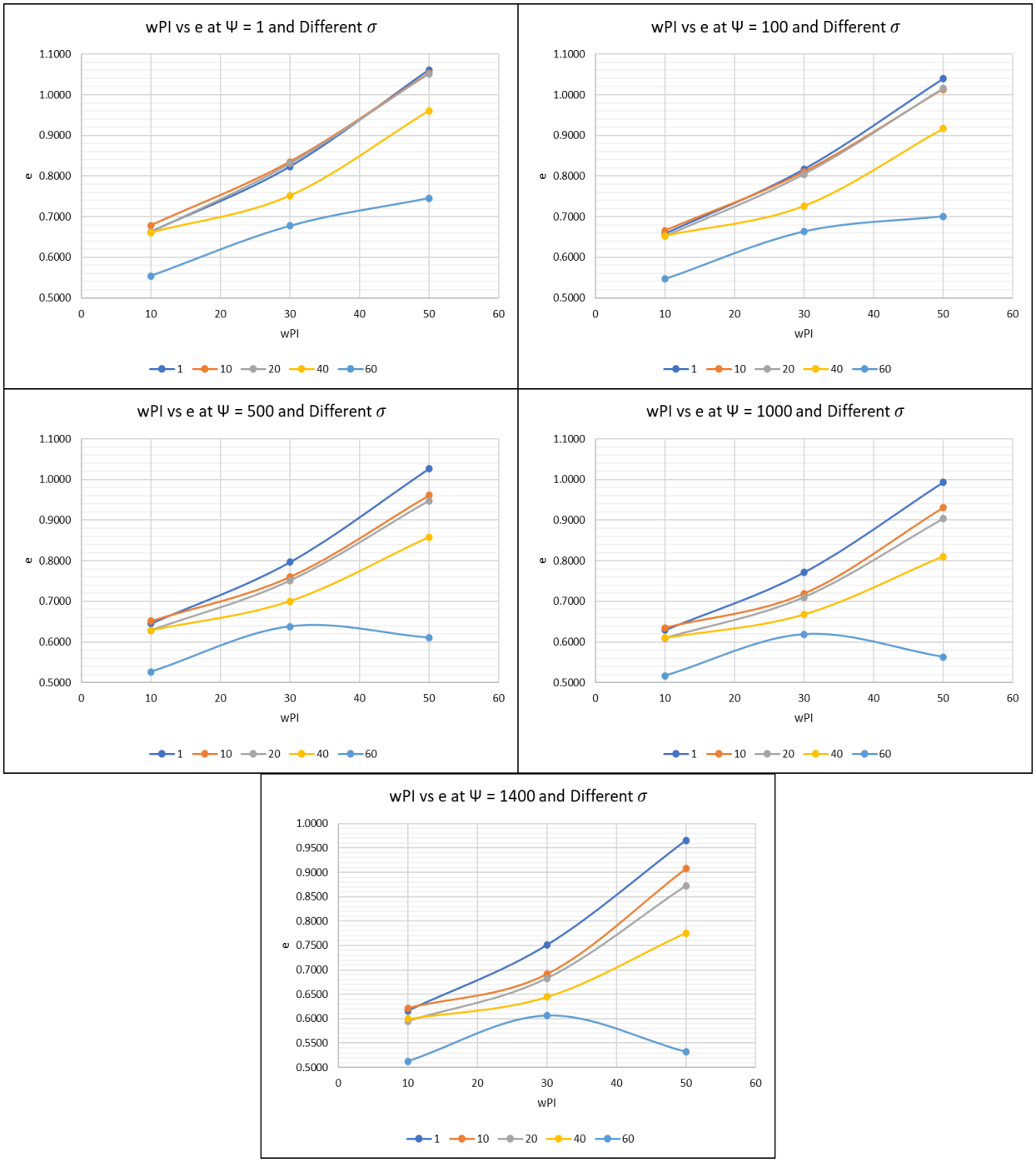

Figure 3A.5 Change in Void Ratio with Respect to Change in *w*PI for Net Normal Stress Values 1, 10, 20, 40, and 60

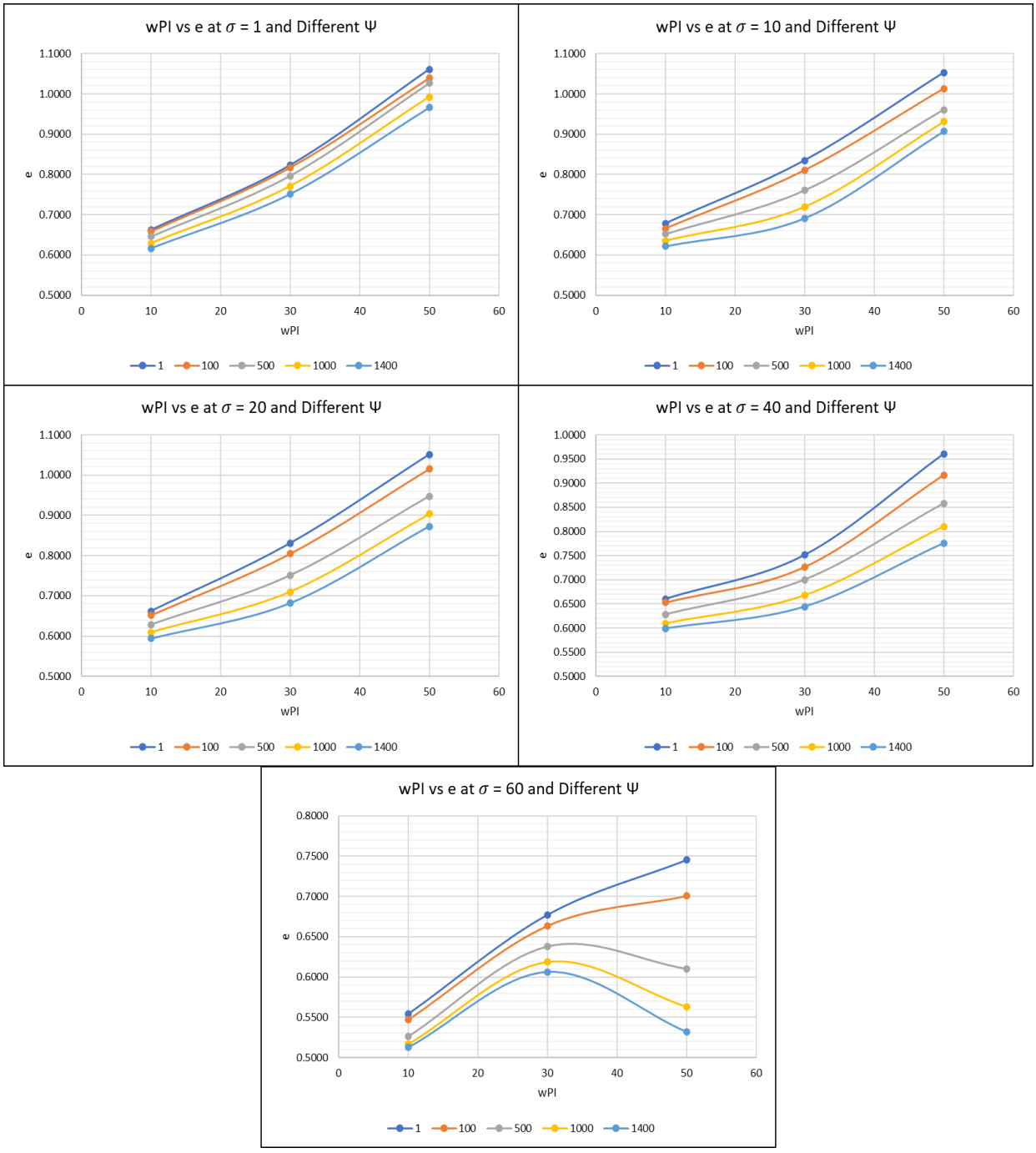

Figure 3A.6 Change in Void Ratio with Respect to Change in *w*PI for Suction Values 1, 100, 500, 1000, and 1400

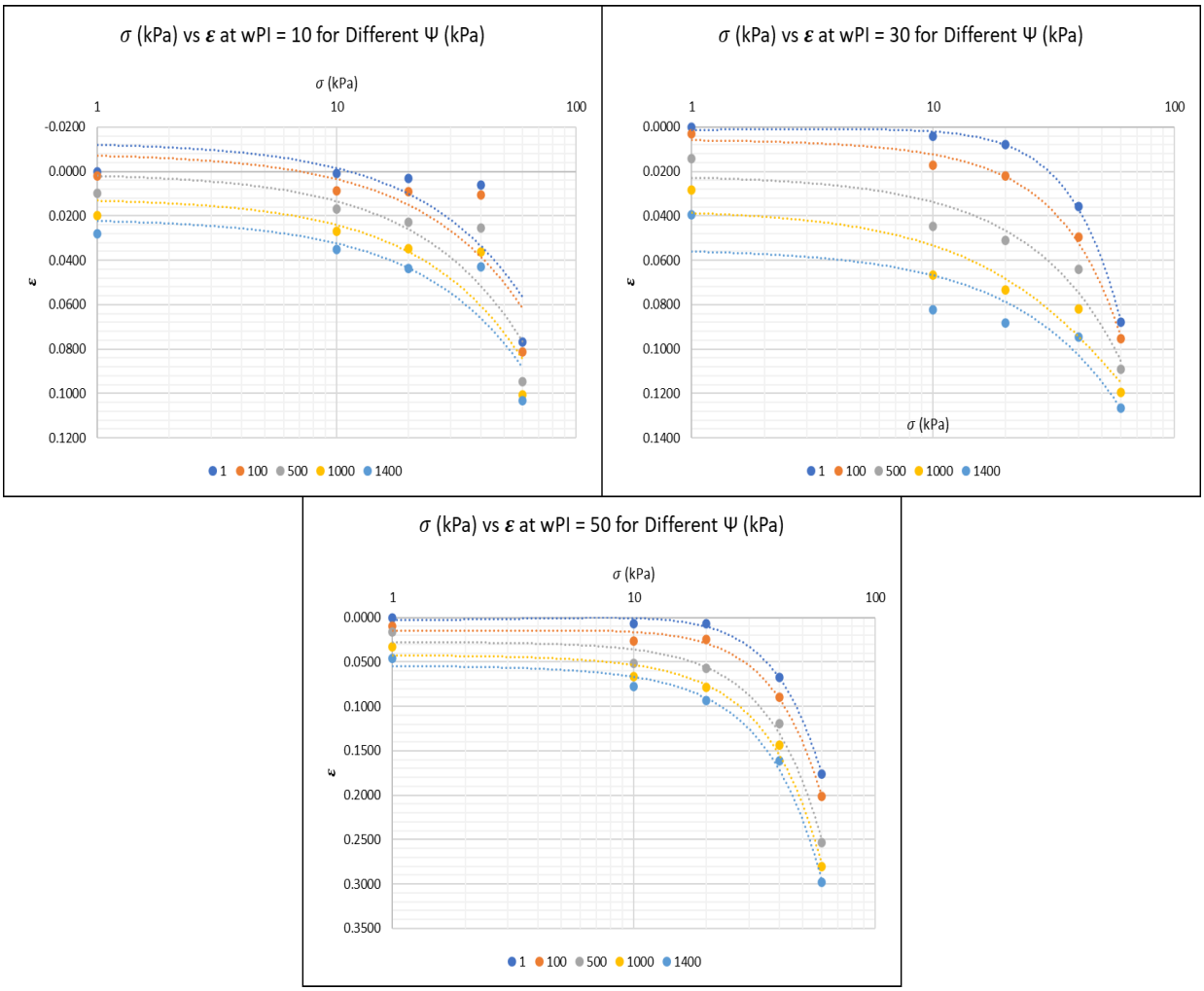

Figure 3A.7 Change in Strain with Respect to Change in Net Normal Stress for Suction Values 1, 100, 500, 1000, and 1400

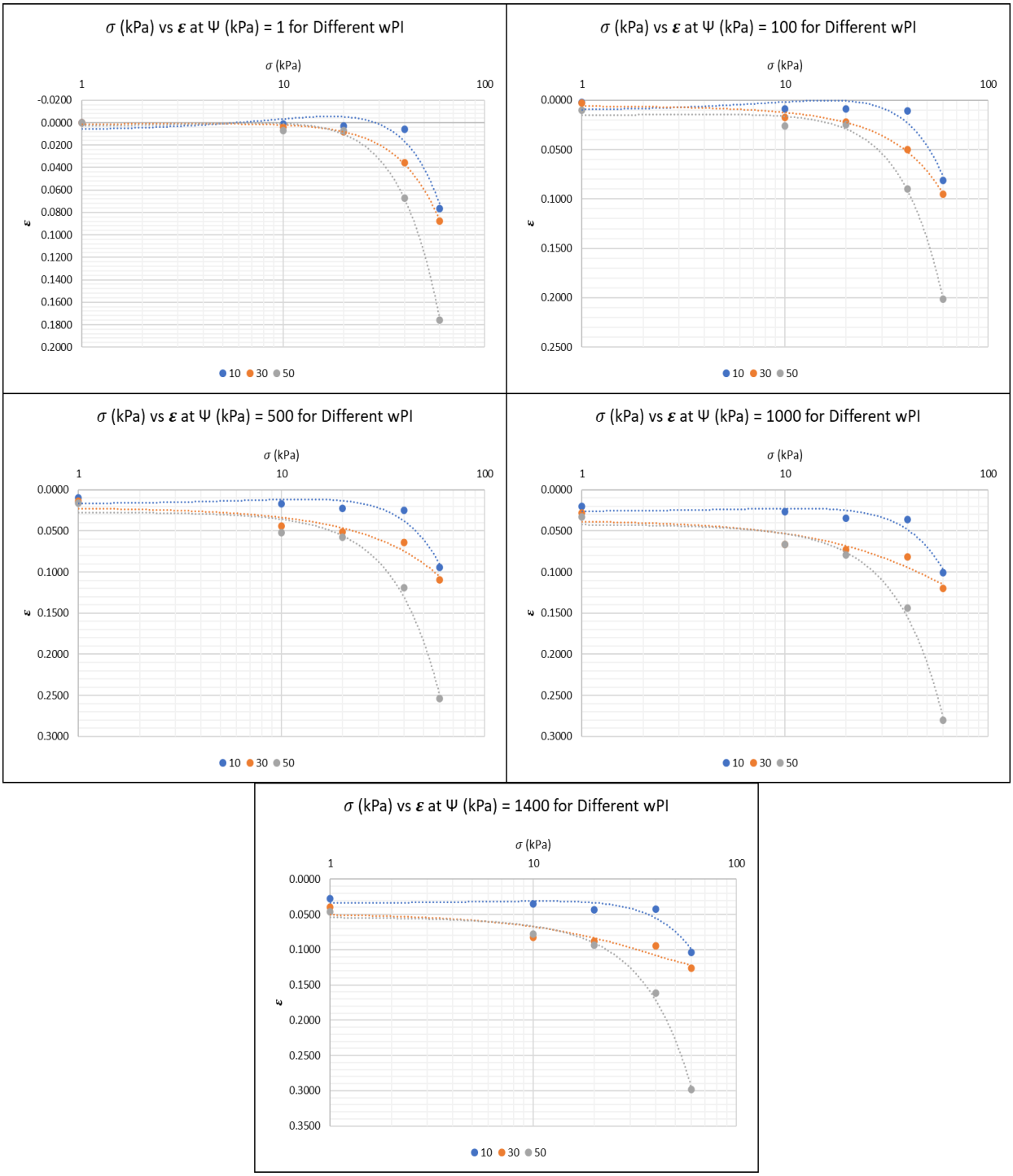

Figure 3A.8 Change in Strain with Respect to Change in Net Normal Stress for *w*PI Values 10, 30, and 50

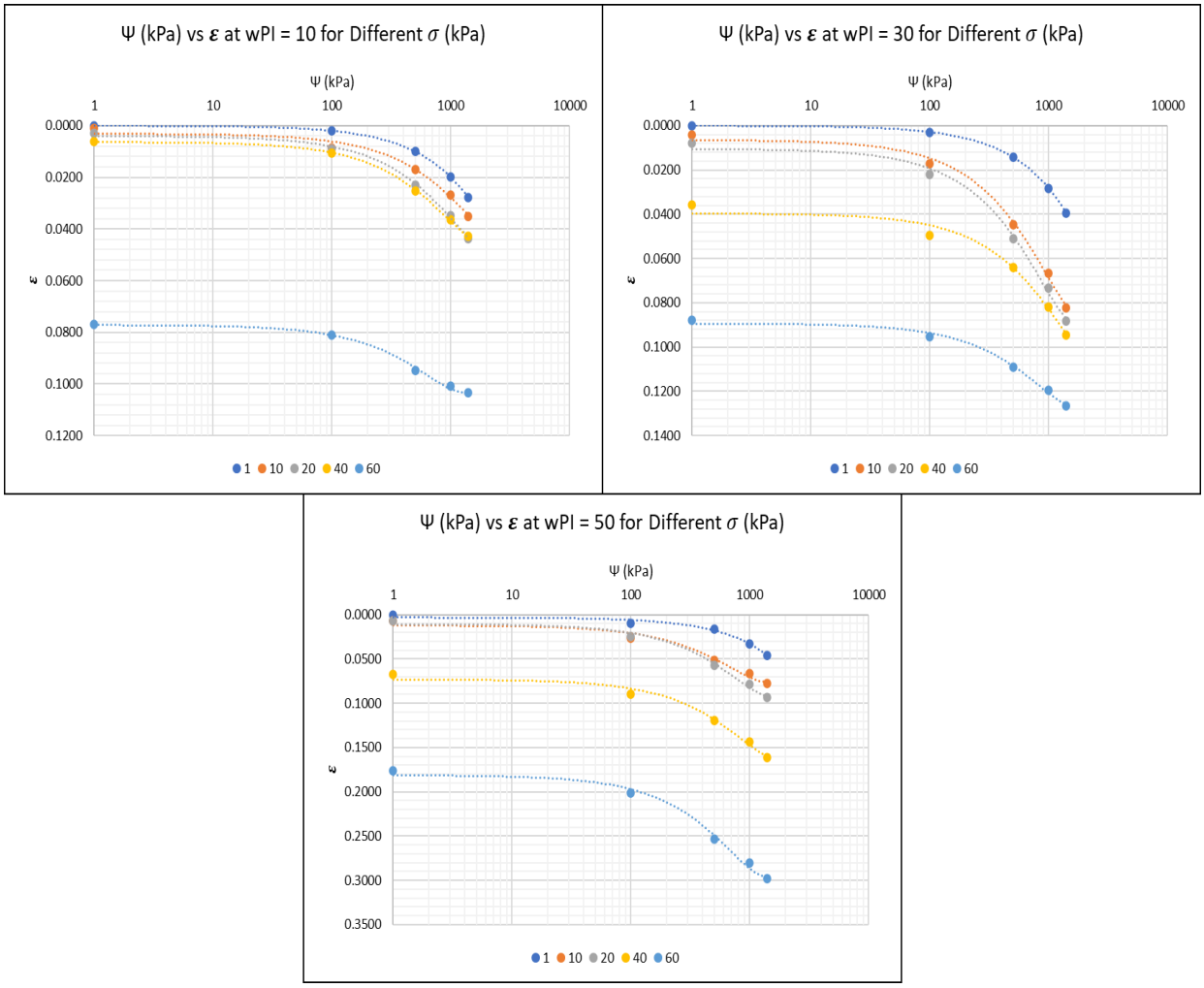

Figure 3A.9 Change in Strain with Respect to Change in Suction for Net Normal Stress Values 1, 10, 20, 40, and 60

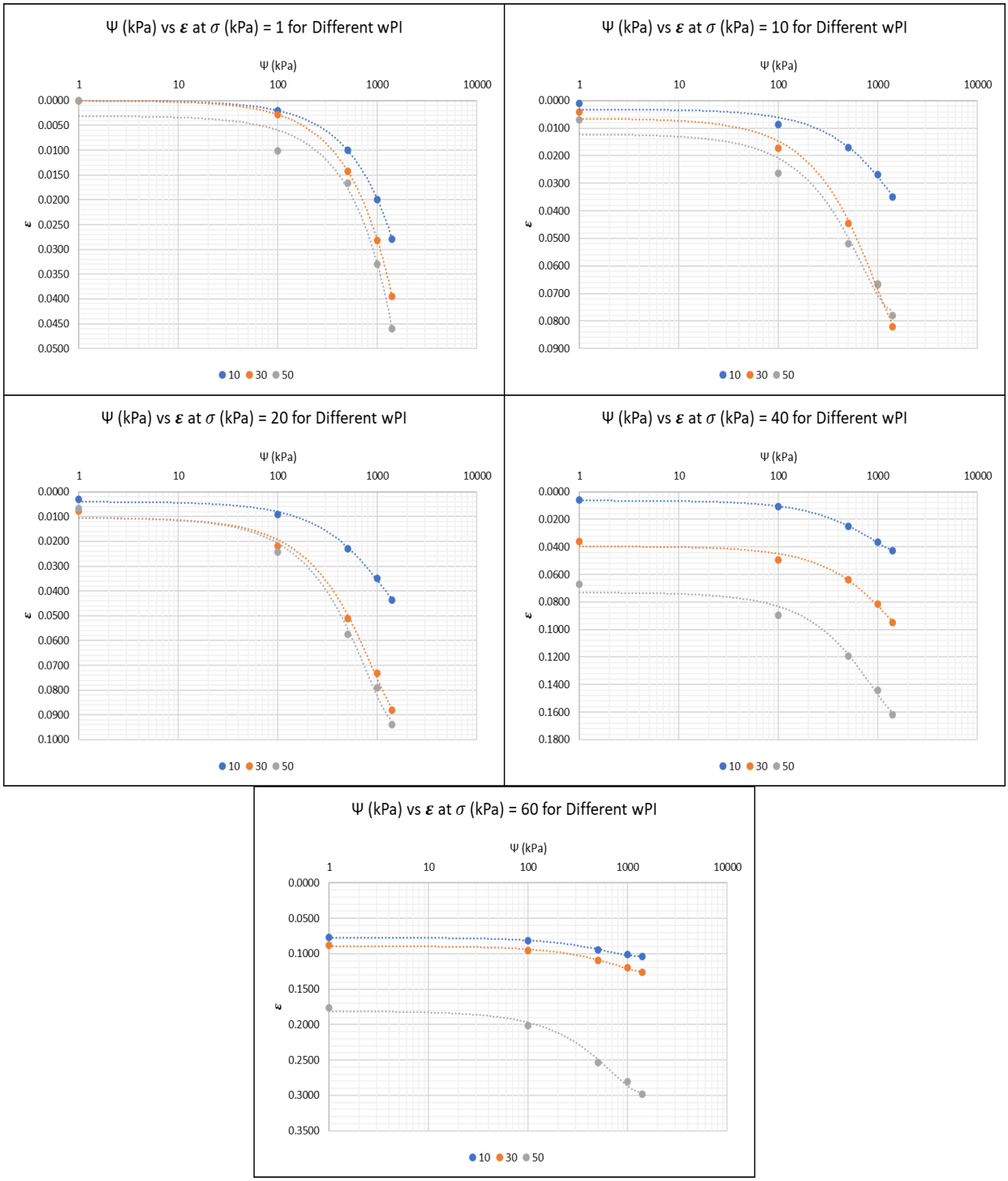

Figure 3A.10 Change in Strain with Respect to Change in Suction for *w*PI Values 10, 30, and 50

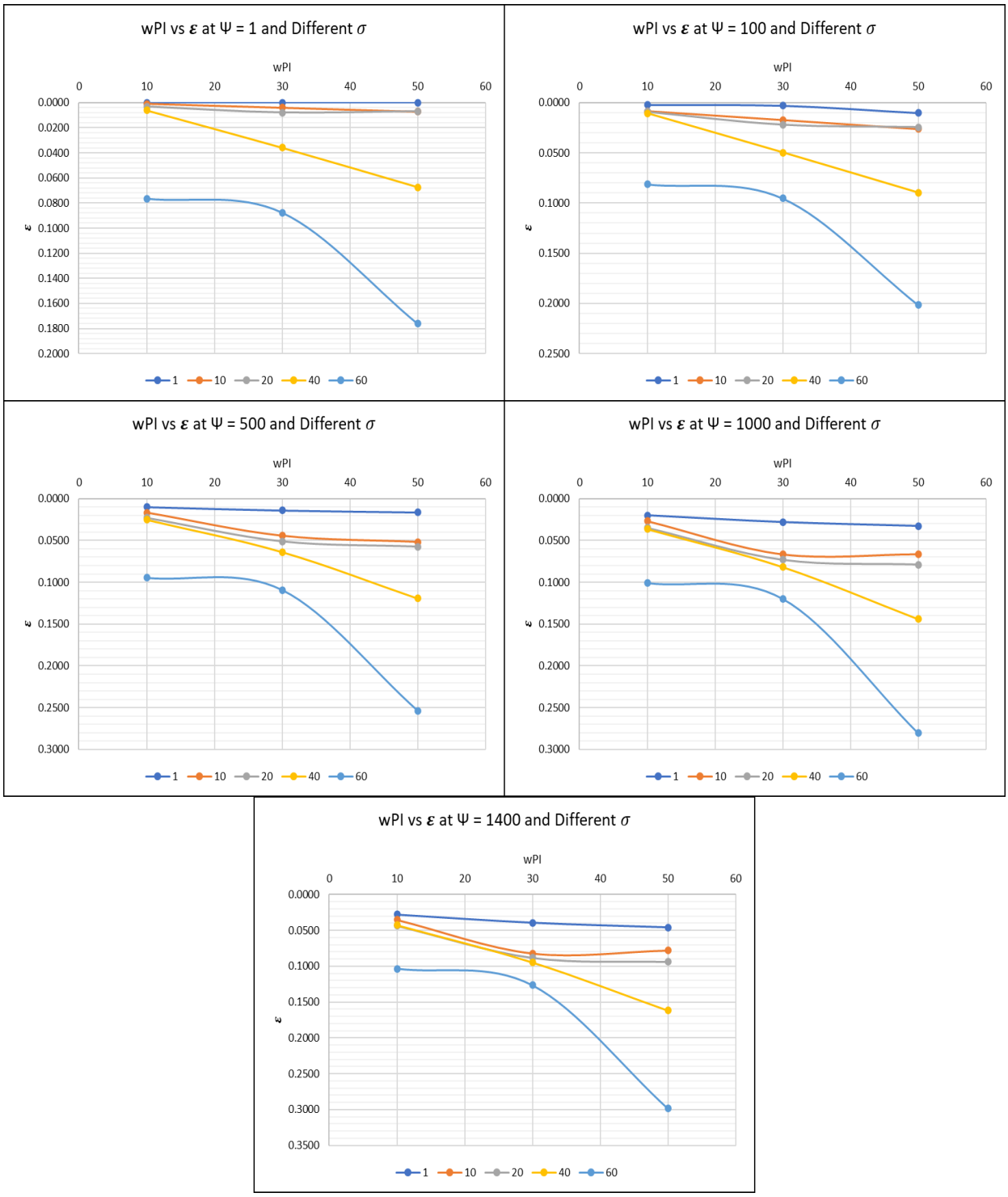

Figure 3A.11 Change in Strain with Respect to Change in *w*PI for Net Normal Stress Values 1, 10, 20, 40, and 60

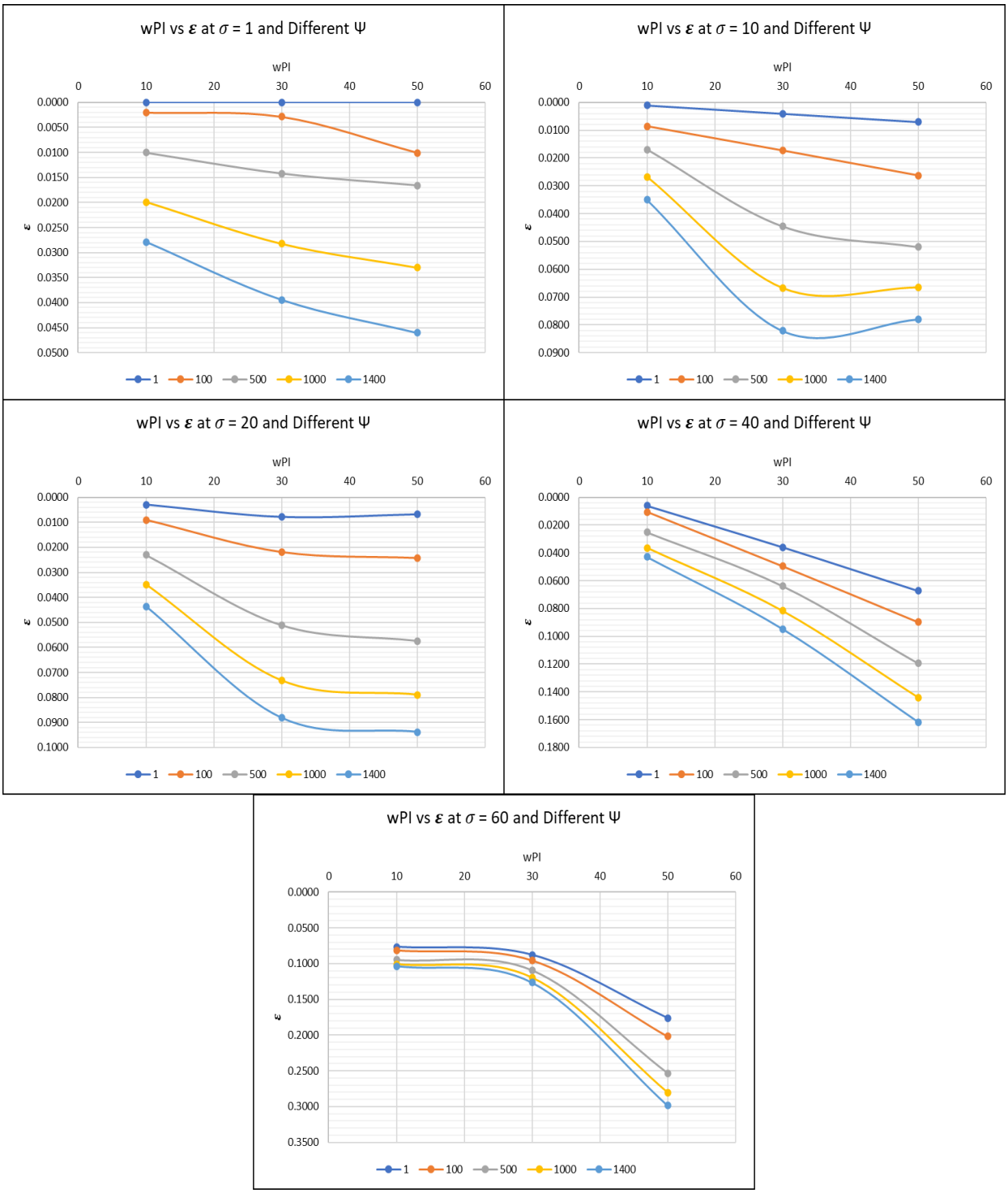

Figure 3A.12 Change in Strain with Respect to Change in *w*PI for Suction Values 1, 100, 500, 1000, and 1400

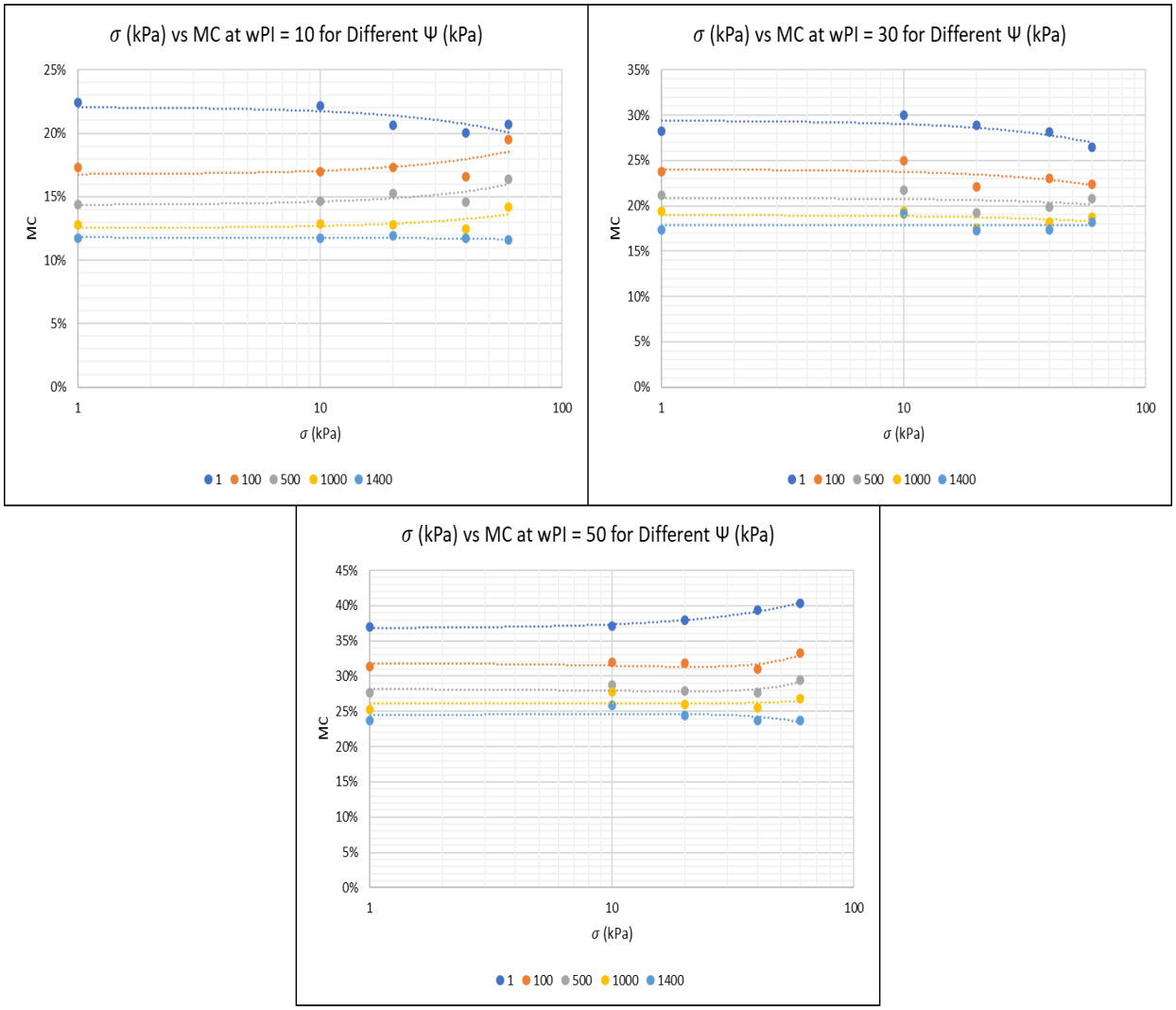

Figure 3A.13 Change in Moisture Content with Respect to Change in Net Normal Stress for Suction Values 1, 100, 500, 1000, and 1400

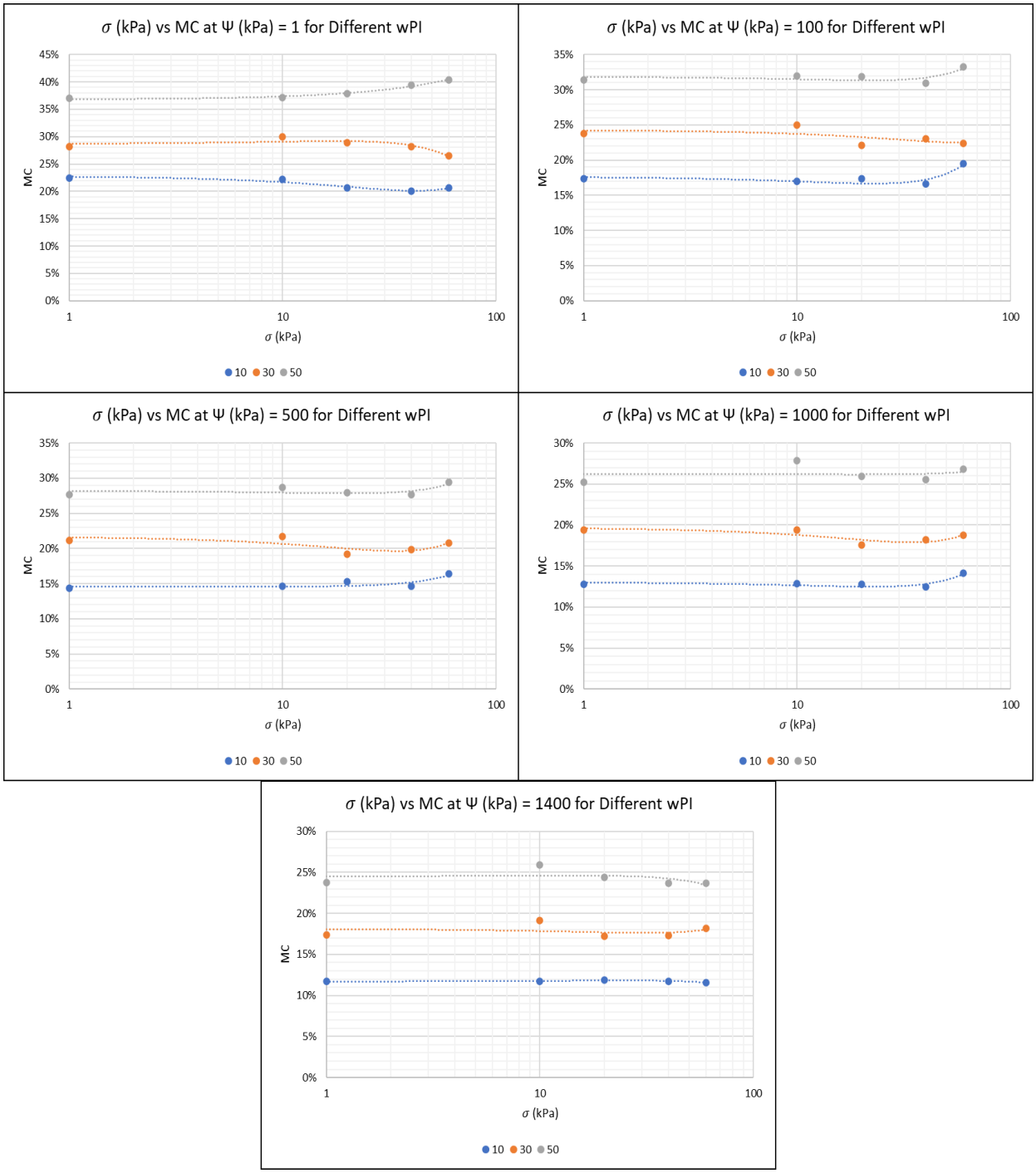

Figure 3A.14 Change in Moisture Content with Respect to Change in Net Normal Stress for *w*PI Values 10, 30, and 50

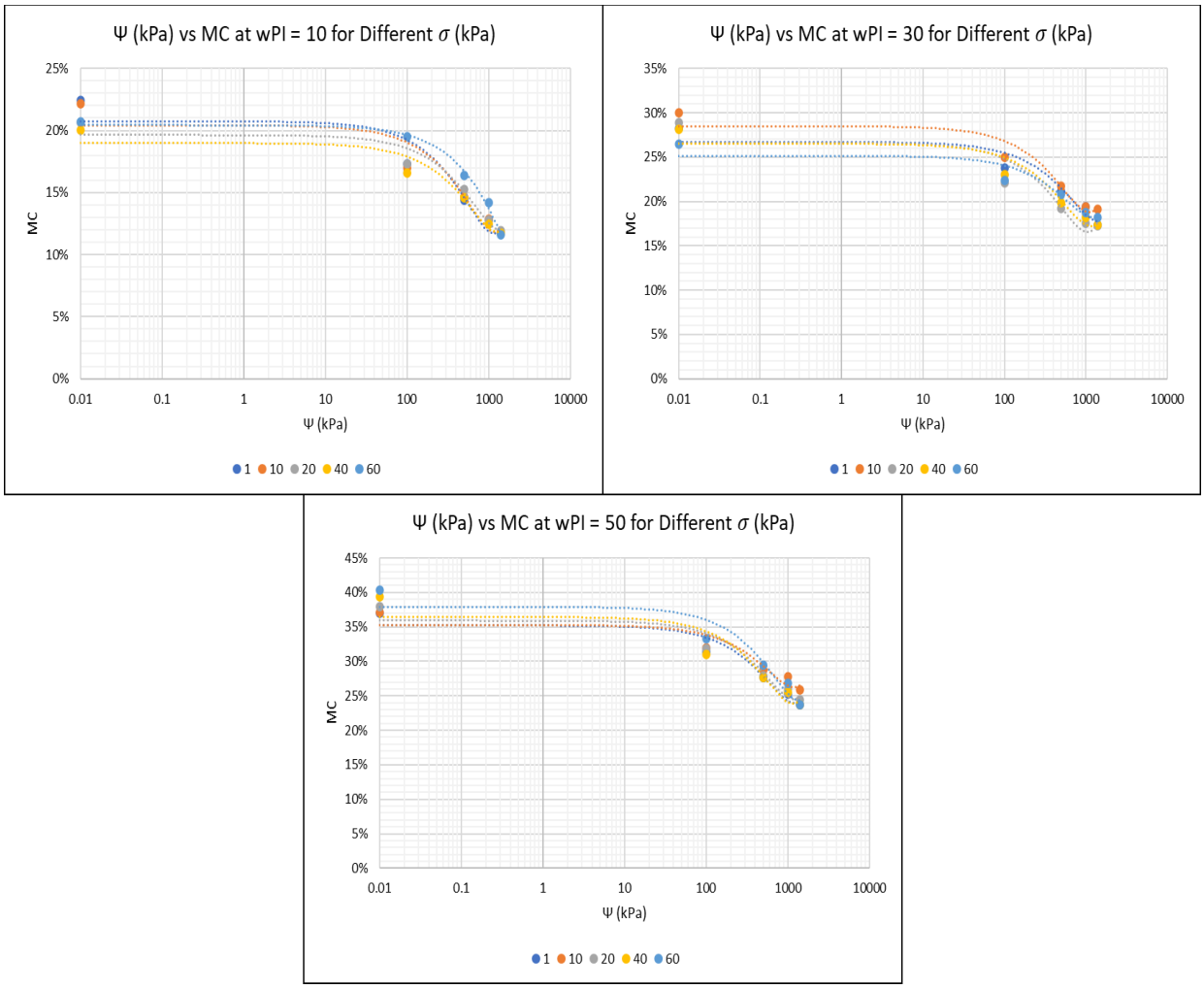

Figure 3A.15 Change in Moisture Content with Respect to Change in Suction for Net Normal Stress Values 1, 10, 20, 40, and 60

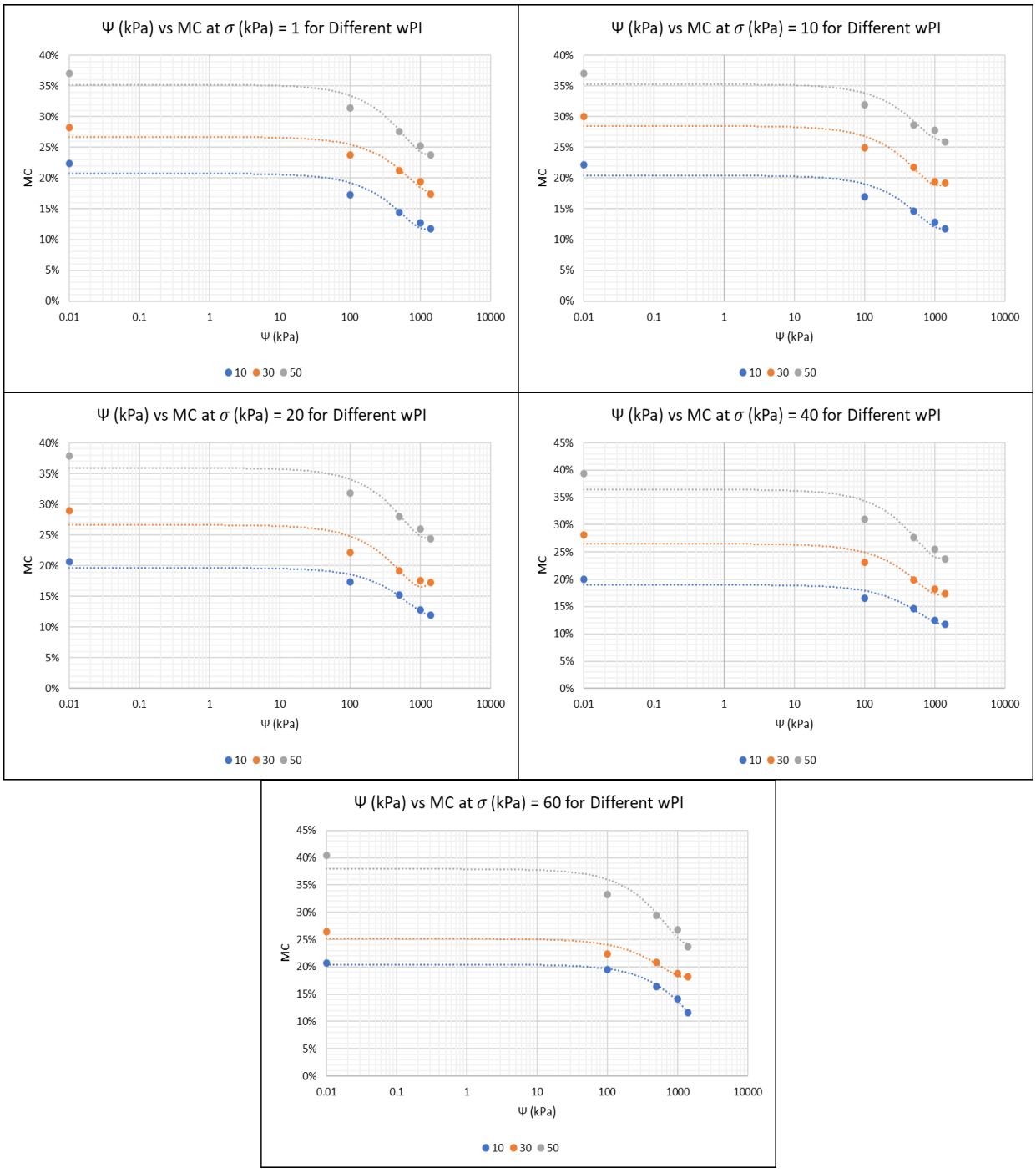

Figure 3A.16 Change in Moisture Content with Respect to Change in Suction for *w*PI Values 10, 30, and 50

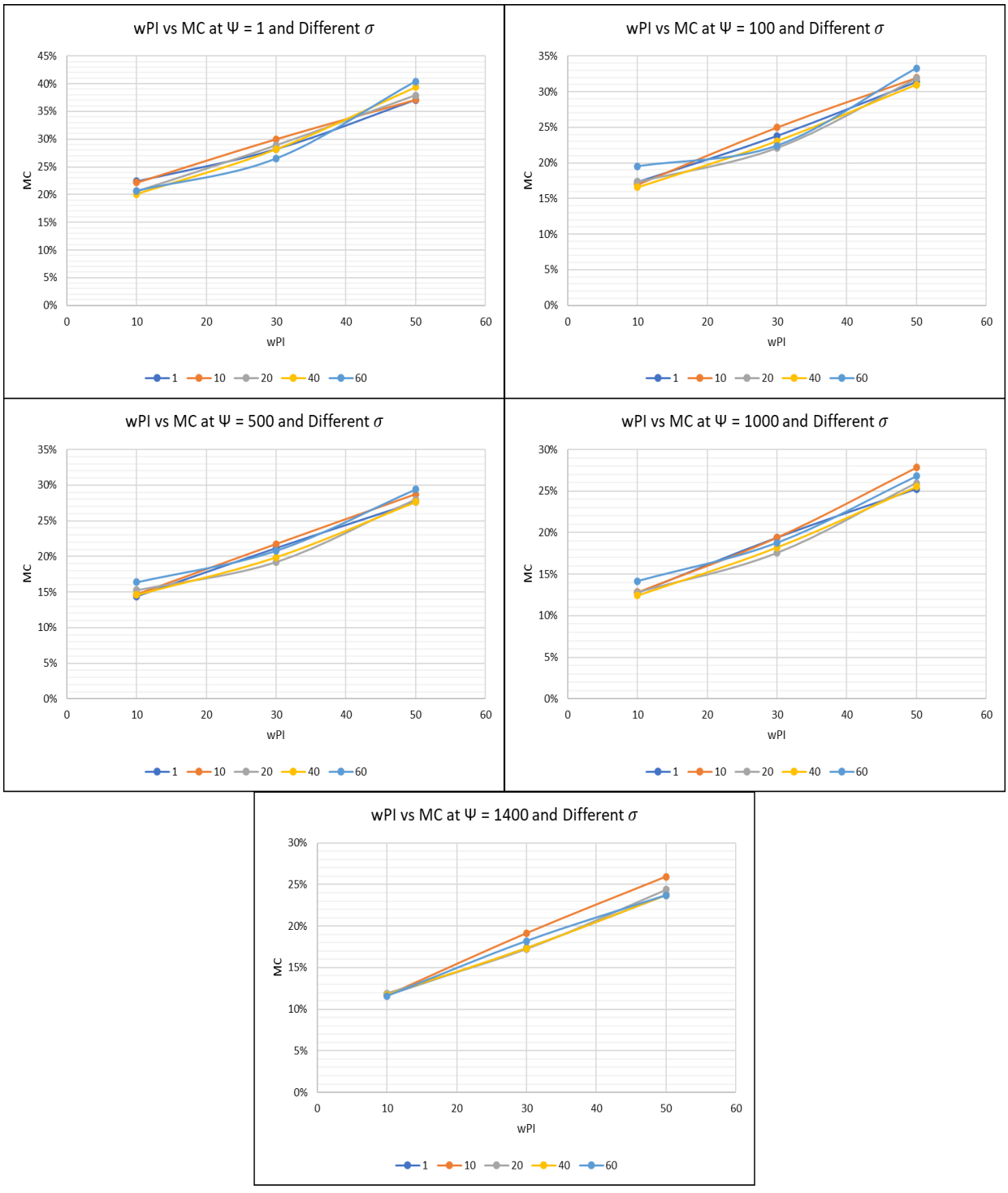

Figure 3A.17 Change in Moisture Content with Respect to Change in *w*PI for Net Normal Stress Values 1, 10, 20, 40, and 60

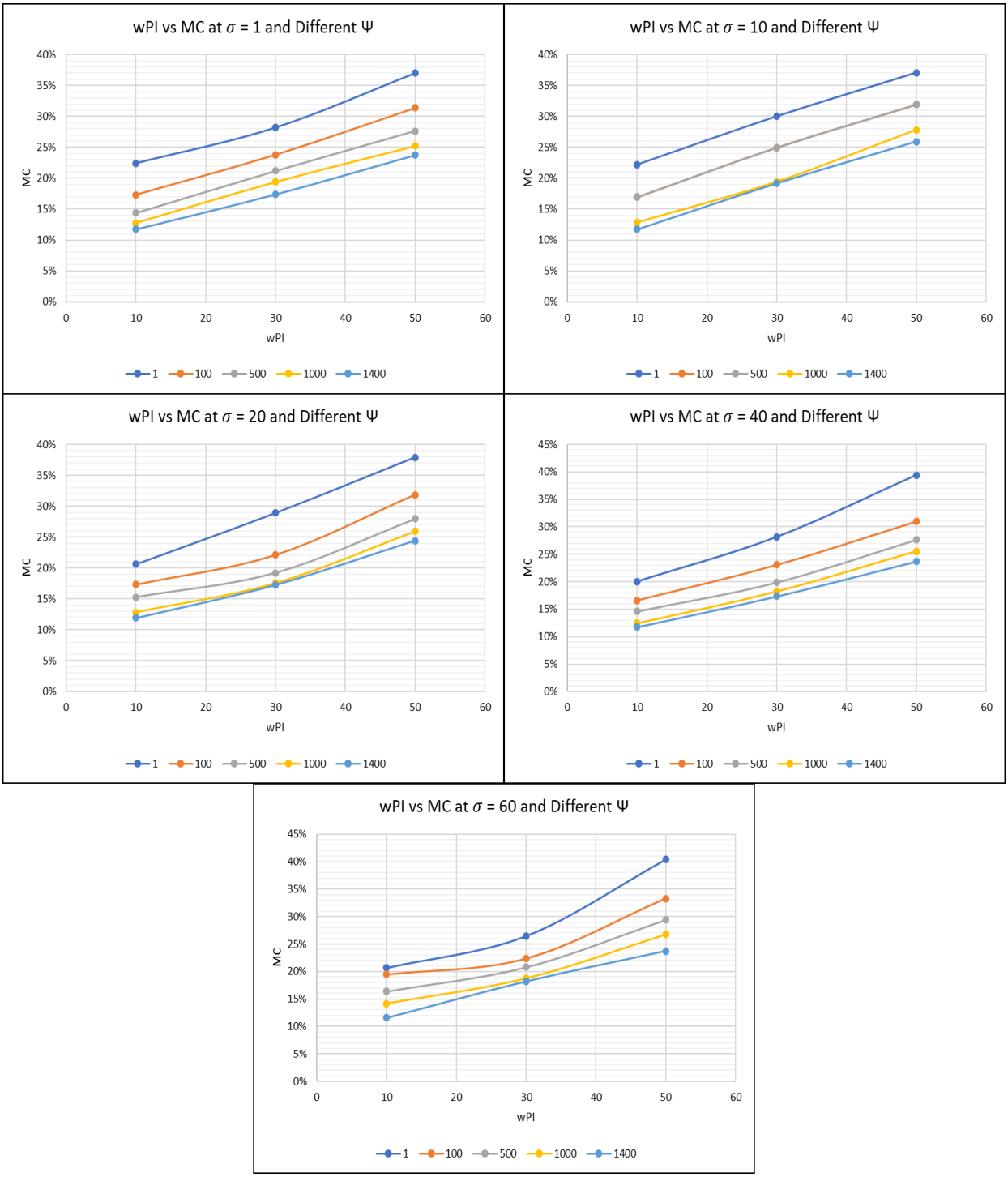

Figure 3A.18 Change in Moisture Content with Respect to Change in *w*PI for Suction Values 1, 100, 500, 1000, and 1400

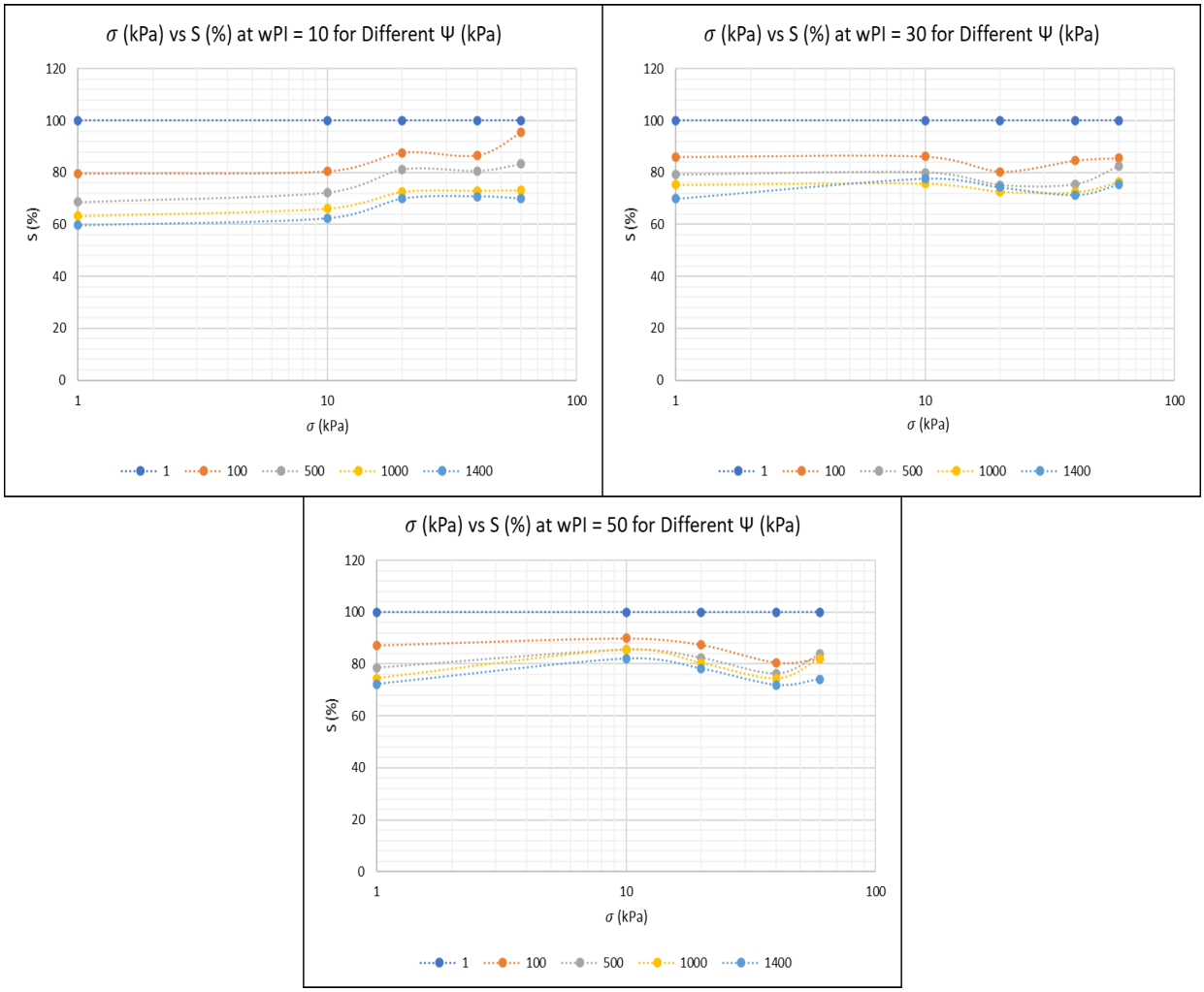

Figure 3A.19 Change in Degree of Saturation with Respect to Change in Net Normal Stress for Suction Values 1, 100, 500, 1000, and 1400

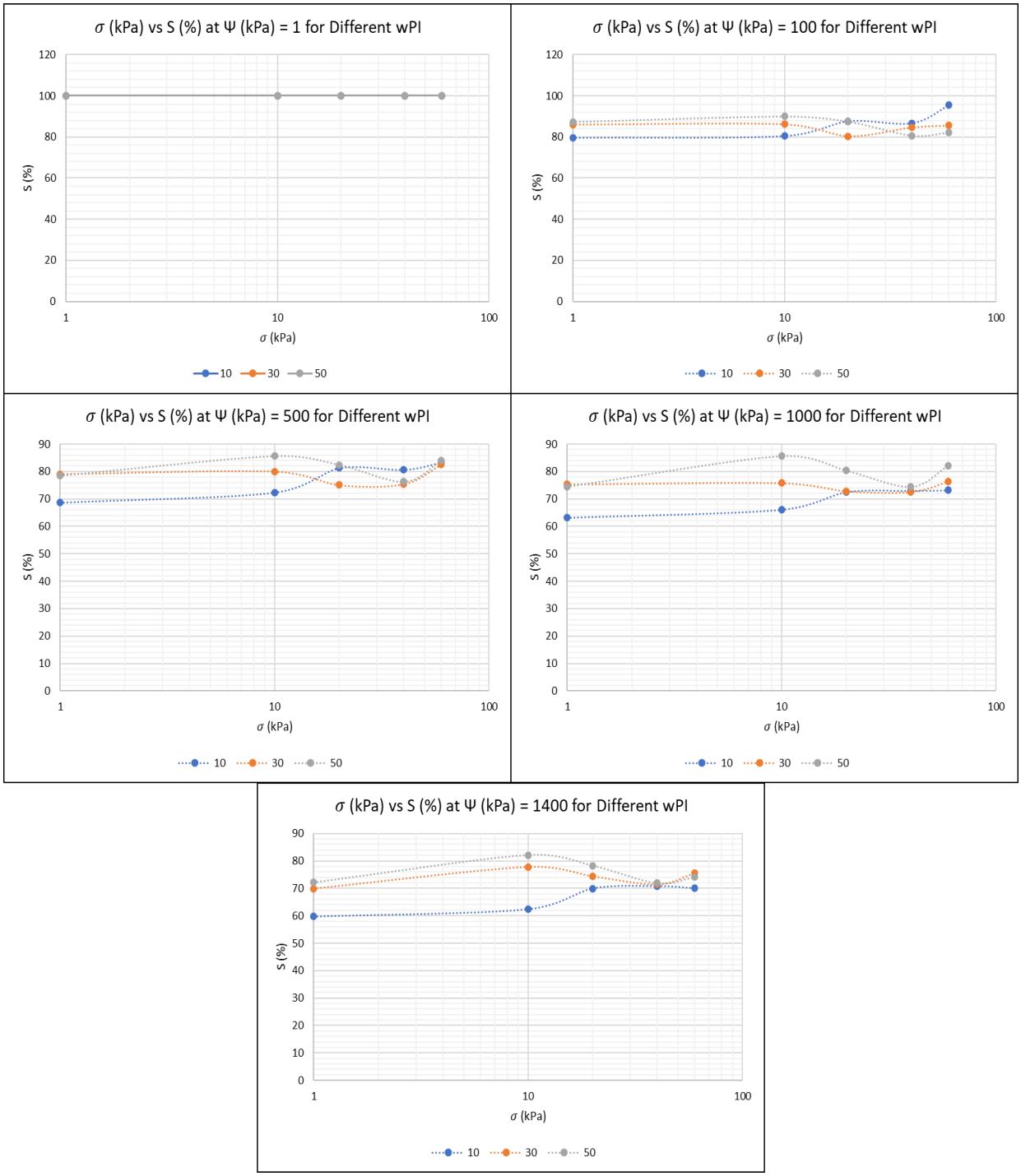

Figure 3A.20 Change in Degree of Saturation with Respect to Change in Net Normal Stress for *w*PI Values 10, 30, and 50

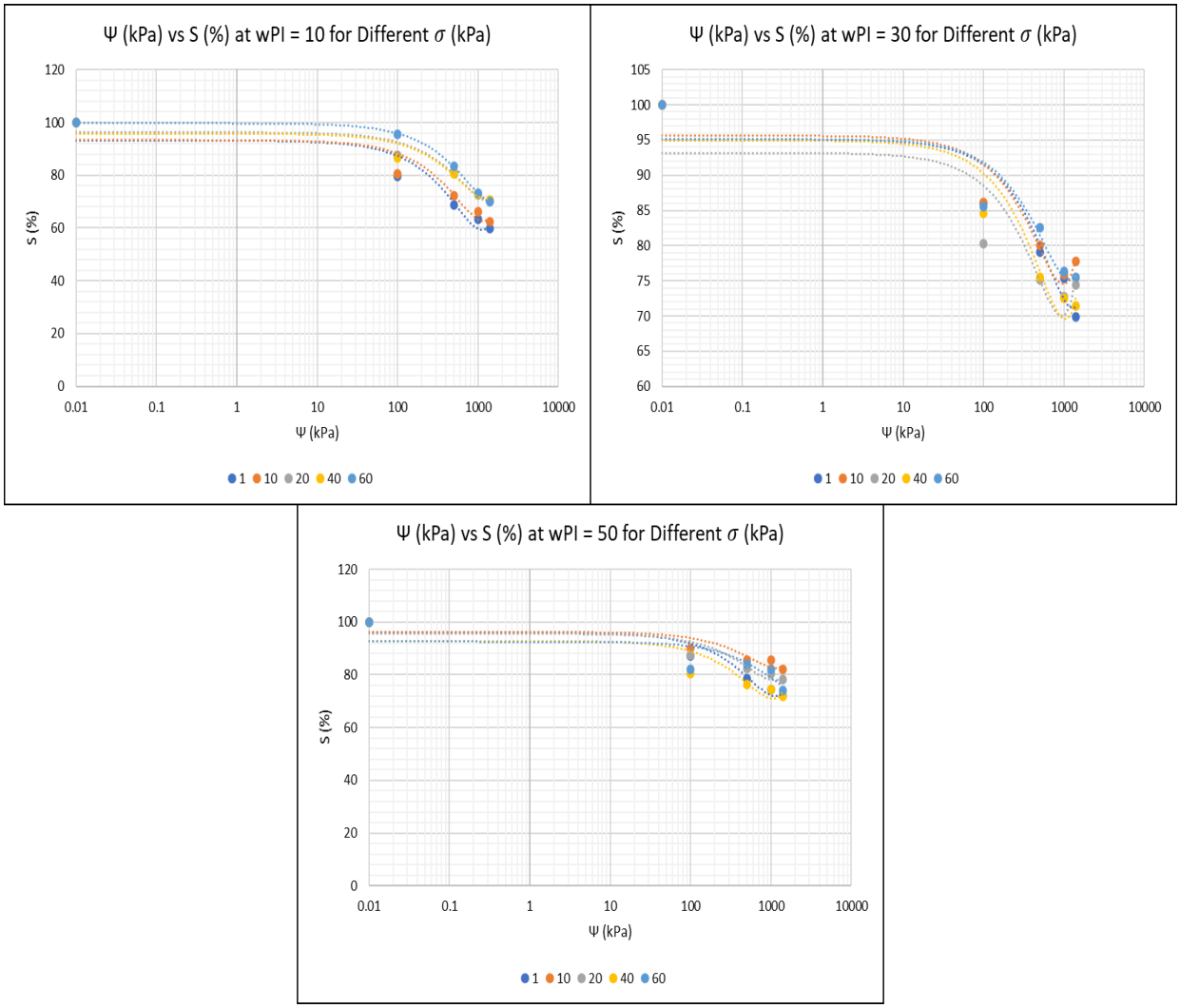

Figure 3A.21 Change in Degree of Saturation with Respect to Change in Suction for Net Normal Stress Values 1, 10, 20, 40, and 60

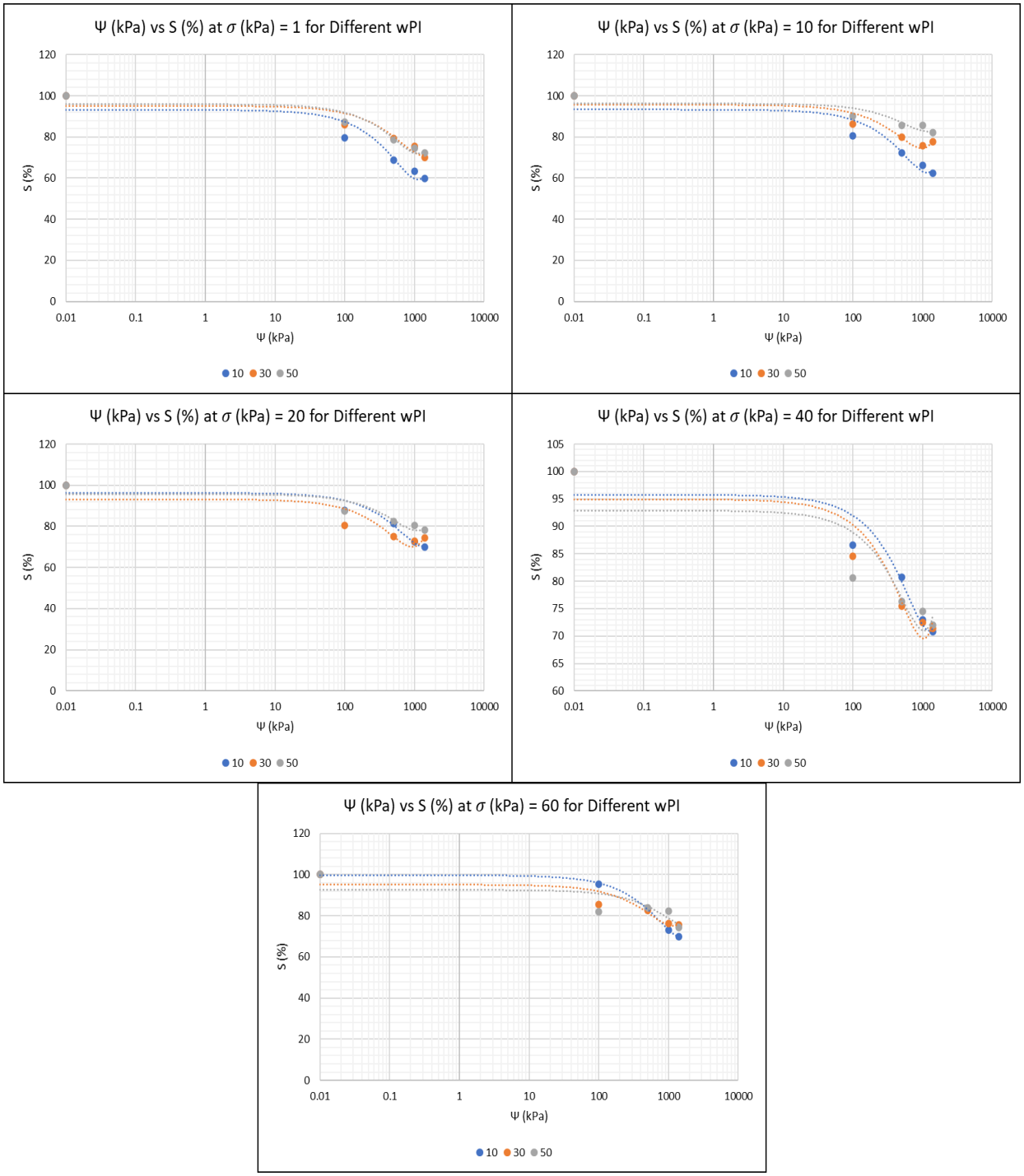

Figure 3A.22 Change in Degree of Saturation with Respect to Change in Suction for *w*PI Values 10, 30, and 50

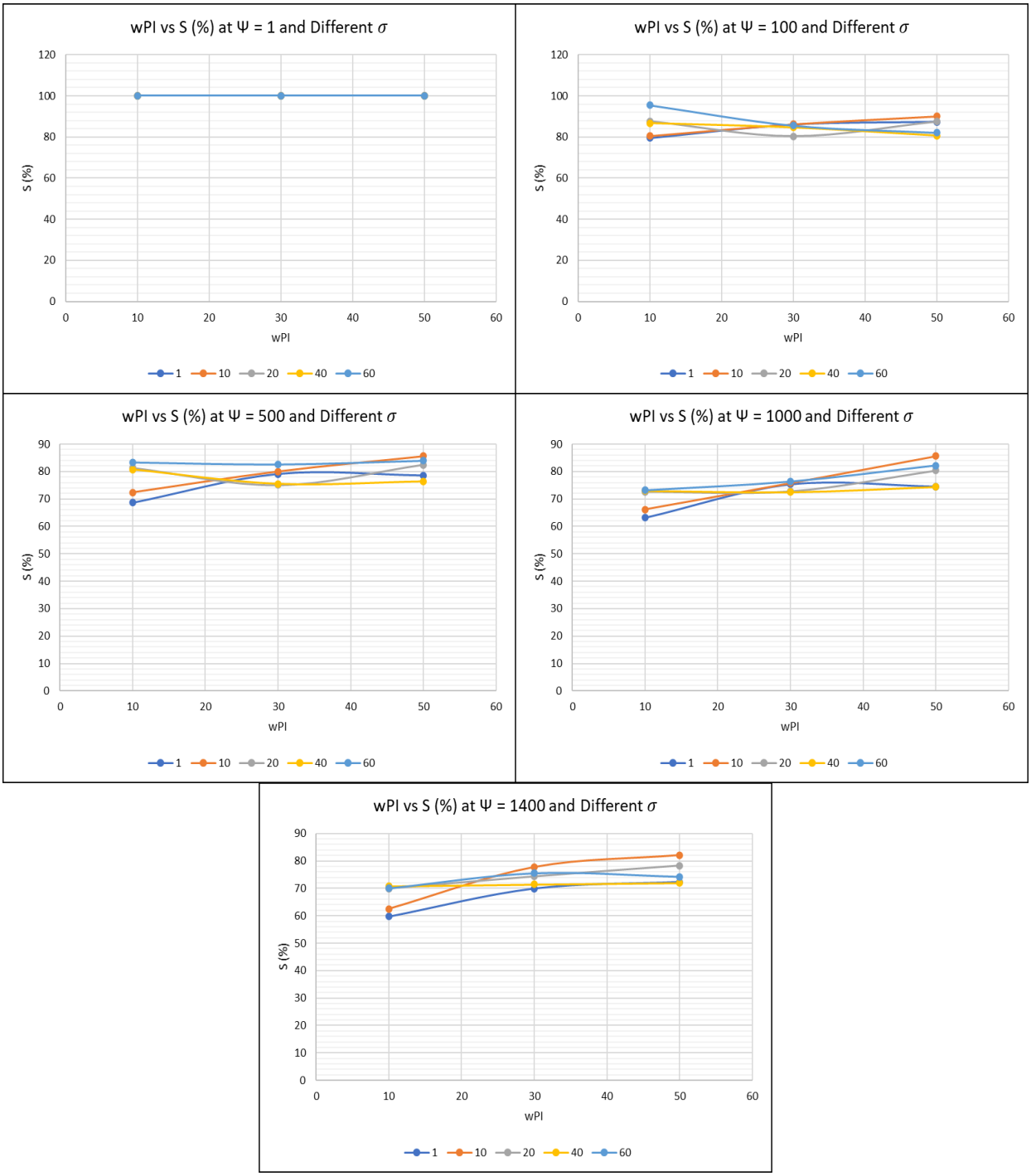

Figure 3A.23 Change in Degree of Saturation with Respect to Change in *w*PI for Net Normal Stress Values 1, 10, 20, 40, and 60

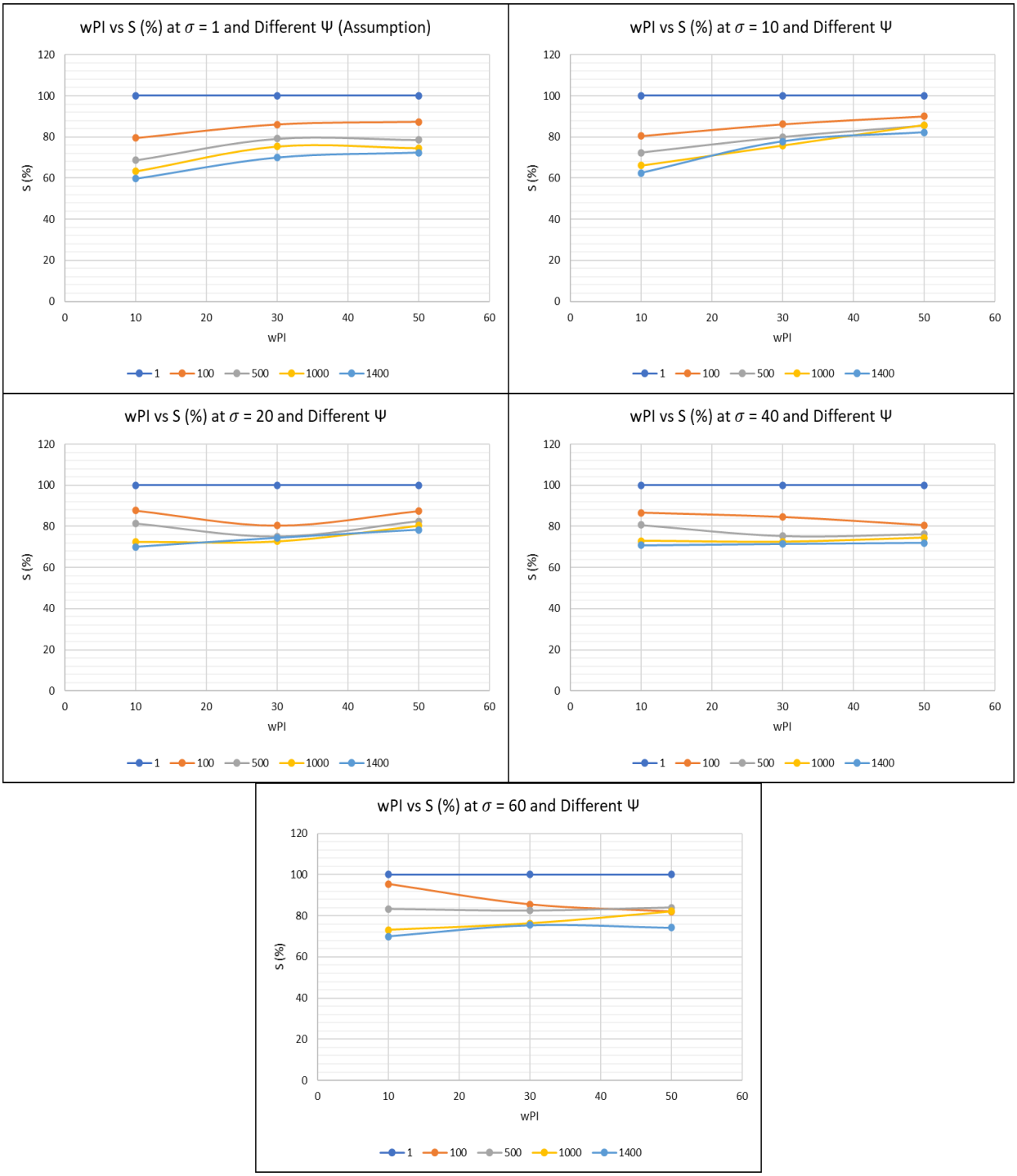

Figure 3A.24 Change in Degree of Saturation with Respect to Change in *w*PI for Suction Values 1, 100, 500, 1000, and 1400